CHALMERS
UNIVERSITY OF TECHNOLOGY

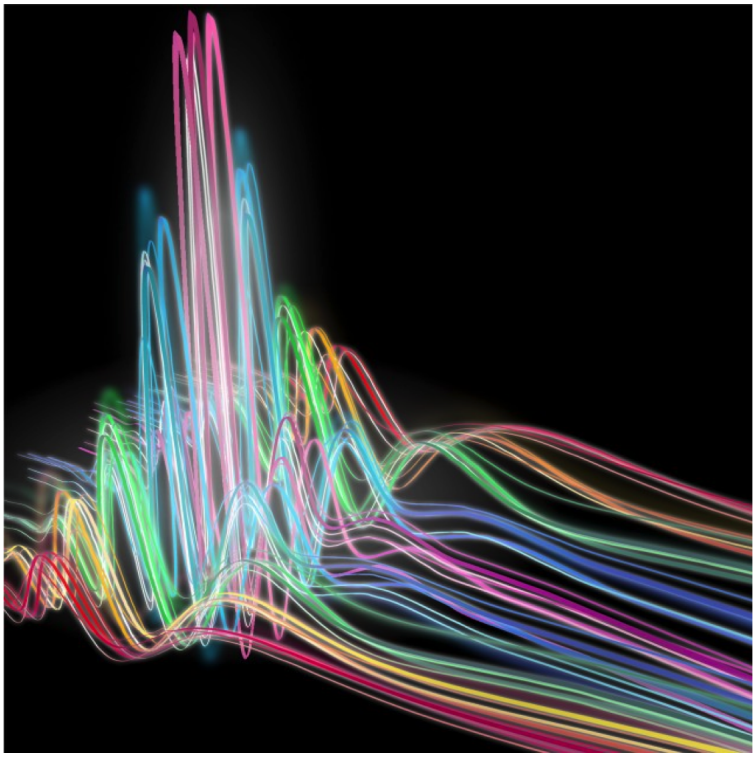

Nonlinear Impedance Spectroscopy

Using higher harmonics response and differential impedance for electrical characterization of DC insulation materials

Master's thesis in Applied Physics

LOUISE ALMQUIST

Department of Materials and Manufacturing Technology
CHALMERS UNIVERSITY OF TECHNOLOGY
Gothenburg, Sweden 2015

Nonlinear Impedance Spectroscopy

Using higher harmonics response and differential impedance for electrical characterization of DC insulation materials

by

LOUISE ALMQUIST

Diploma work No. 170/2015
Department of Materials and Manufacturing Technology
CHALMERS UNIVERSITY OF TECHNOLOGY
Gothenburg, Sweden

Diploma work in the Master programme Applied Physics.

Performed at: ABB Corporate Research
CH - 5405, Baden-Dättwil, Switzerland
Financed by ABB Switzerland Ltd.

Supervisor: Dr. Thomas Christen
ABB Switzerland Ltd.

Examiner: Professor Dr. Stanislaw Gubanski
Department of Materials and Manufacturing Technology
Chalmers University of Technology, SE - 412 96 Gothenburg

Nonlinear Impedance Spectroscopy
Using higher harmonics response and differential impedance for electrical characterization of DC insulation materials
LOUISE ALMQUIST

Diploma work no 170/2015
Department of Materials and Manufacturing Technology
Chalmers University of Technology
SE-412 96 Gothenburg
Sweden
Telephone + 46 (0)31-772 1000

Cover: Illustration of higher harmonics generation: Tenio Popmintchev and Brad Baxley, JILA/University of Colorado, *Artist's impression of high-harmonic generation: turning a single infrared frequency of light into thousands of new frequencies, including X-rays*. 2012.

Printed by [Reproservice]
Gothenburg, Sweden 2015

Nonlinear impedance spectroscopy
Using higher harmonics response and differential impedance for electrical characterization of DC insulation materials

LOUISE ALMQUIST
Department of Materials and Manufacturing Technology
Chalmers University of Technology

Abstract

With the growing relevance of high-voltage direct current (HVDC) technologies comes an increased need of reliable electrical characterization of insulation materials. Electrical conduction mechanisms in insulation materials under DC voltages are rather complicated and appropriate characterization tools need to be further developed. This thesis investigates the potential of using nonlinear impedance spectroscopy (IS) for electrical characterization of insulation materials at DC fields, or at low frequency AC fields. A theoretical background is provided where it is shown for different models how nonlinear current-field dependence give rise to currents that contain amplitudes at higher frequencies than that of the exciting voltage (the fundamental frequency). Experimentally, different material systems were studied with two advanced nonlinear IS measurement techniques; higher harmonics measurements at high fields and differential conductivity measurements with small amplitude AC spectroscopy at large superimposed DC. The main results are presented in form of steady state current-field characteristics. Figure 5.3 and 5.9 show, for two different robust material systems, that results from the two IS methods are in close agreement with each other and with two other setups used for consistency check. We therefore conclude that nonlinear IS is in principle useful for electrical characterization of nonlinear insulation materials, particularly field grading materials. Limitations of the methods are related to non-robust material properties and problems with reaching a quasi-steady state at reasonable frequencies.

Keywords: HVDC insulation, impedance spectroscopy, dielectric spectroscopy, nonlinear materials, field grading.

Acknowledgements

This thesis was a part of a larger project at ABB Corporate Research in Switzerland and was performed in a team, consisting of myself, my supervisor Thomas Christen and Roman Kochetov. Foremost, I would like to express my deepest gratitude to Thomas Christen for his excellent guidance, immense knowledge, patience and enthusiasm. He was a great source of inspiration and I could not have imagined having a better supervisor. Special thanks also to Roman Kochetov for his guidance in the lab and for his help with carrying out experiments. I truly appreciate his help and his insightful comments. I would also like to acknowledge all my other colleagues at ABB for making the days at work, and my stay in Switzerland, very fun and memorable. My sincere thanks also to Prof. Stanislaw Gubanski for his support and valuable feedback. Last but not the least, I would like to thank my family and friends for their encouragement during my entire studies.

Louise Almquist, Gothenburg, December 2015

Contents

List of Figures

List of Tables

1

Introduction

The electric power market is changing due to a growing demand for renewable energy. Since generation equipment of renewable energy, like wind farms and solar power plants, seldom are located near to places where the power is needed, novel electricity technologies are developed. High-voltage direct current (HVDC) technology is expected to grow far beyond its traditional position as a supplement to alternating current (AC) transmission. Consequently, the need of appropriate insulation materials for HVDC applications is increasing. In the process of developing direct current (DC) insulation materials, reliable characterization methods are needed for the determination of their electrical properties and conduction behaviour at DC fields.

Unfortunately, electrical conduction mechanisms in technical insulation materials at DC voltages, or at low-frequency AC voltages, are rather complicated and difficult to understand. A good general overview can be found in [1]. Due to the physical complexity (different possible carrier types, different possible transport mechanisms, contact effects, etc.) and the consequent lack of robustness [2] a set of different experimental tools is needed for a reasonable electrical characterization of the materials. One such tool is impedance spectroscopy (IS), also called dielectric spectroscopy (DS).

Impedance spectroscopy is nowadays standard for characterizing dielectric materials used in AC applications [3, 4]. However, DC fields can lead to conduction behaviour which is only observable at very low frequencies and at sufficiently high electric fields. Broadband impedance spectroscopy [5] allows the study of dielectric properties in the low frequency region. This thesis focuses on the potential of using high voltage broadband impedance spectroscopy for DC characterization of nonlinear insulation materials [6, 7].

1.1 Modern broadband impedance spectroscopy

Traditional IS or dielectric spectroscopy (the terms will be used synonymously) is based on linear response theory, where the current response is measured for small amplitude excitations of the applied harmonically oscillating voltage. The frequency of this harmonic excitation is called the "fundamental frequency". The linear response

has then the same frequency, and in general also a phase shift. Modern IS equipment can go to higher voltages and thus into the nonlinear region, and can thereby provide additional information on the conduction mechanisms at higher fields. For larger excitation voltages, the current response can contain amplitudes at higher frequencies than that of the fundamental frequency. As we will see, such higher harmonics ("superharmonics") are generated by nonlinearities.

Three types of IS measurements are in the focus in this thesis:

1. Small signal IS (linear response): Measurements in large frequency ranges ($10^{-4} - 10^{6}\,\mathrm{Hz}$) at low AC voltage ($\mathrm{U_{rms}} = 1\,\mathrm{V}$), where the low-frequency region is of most interest for our purpose. The quantities of interest are the frequency dependent permittivity and conductivity, or combinations of them (like the loss angle etc.).

2. High-Voltage IS: Measurements of higher harmonics. These measurements are performed at rather high AC voltage amplitudes (up to $\mathrm{U_{rms}} = 1414\,\mathrm{V}$).

3. Superimposed DC-AC IS: Measurements of the current response to an (often small) AC voltage superimposed to an (often large) DC voltage. This type of measurement makes it possible to probe dynamic and static properties along the steady-state current-voltage characteristics, like e.g. the differential conductivity.

The two latter measurement techniques refer to 'nonlinear dielectric spectroscopy' in our terminology.

Methods that enable nonlinear spectroscopy have already been developed and applied to a variety of materials, such as liquid crystals and solid ferroelectrics [8]. Measurements of higher harmonics have also been performed on field grading materials before [9, 10]. Nonlinear IS has been also been used at low frequencies for comparison with DC field experiments and theoretical results [11]. However, research where IS is used to study the DC behaviour of material systems is very limited and needs to be understood better.

1.2 Aim of this study

The aim of this work is to contribute to the understanding and to the application of nonlinear IS techniques for material characterization. More specific, the aims are to elaborate the potential and to work out the concept of measurement type 2 and 3 in the previous section as part of the material characterization for HVDC applications. Focus will be more on the conduction current part, and less on nonlinearities in the electric displacement.

Important parts are the theoretical understanding, experimental feasibility and limits, elaborating ways of representation, analysis of the measurements and in particular, consistency between the different approaches.

1.3 Structure of the thesis

The next chapter provides parts of the fundamental theory. The principles of both linear and nonlinear dielectric spectroscopy are explained and several theoretical model examples are provided for a deeper understanding of nonlinearities and higher harmonics. Thereafter, a chapter explaining the experimental equipments is provided. Subsecquently, different model material systems that were studied are introduced. The experimental results are then presented for the considered material systems. Finally, the results are discussed and some conclusions are drawn.

2

Theory

In this chapter the fundamental theory underlying this thesis is provided, starting with an overview on linear dielectric spectroscopy. Thereafter the concept of nonlinearities and superharmonics is explained, including several examples of electric nonlinear behaviour. Finally, differential spectroscopy is introduced, where a small signal AC voltage is superimposed to a DC voltage. Before going into the theory sections mentioned, some general remarks that are necessary for a correct interpretation of this work are explained.

Firstly, in all the experimental and theoretical investigations only plane plate samples are considered. In IS measurements the system (a single plate or a series of different plates) under investigation is positioned between two metal electrodes, see figure 2.1a. Here L is the total sample thickness and A is the area of the electrode, which is relevant for the current flow. In a Cartesian coordinate system only the dimension perpendicular to the plane of the sample-electrode interfaces, x, has been taken into consideration. In the same figure the equivalent electric circuit is shown, see figure 2.1b, with a conduction current flowing through the resistance and a displacement current over the capacitance. Included for completeness is a series resistance R_0 which is part of the (high voltage) IS measurement circuit in the equipment. It can become relevant at large currents, e.g. at very high frequencies, but will only be considered if necessary.

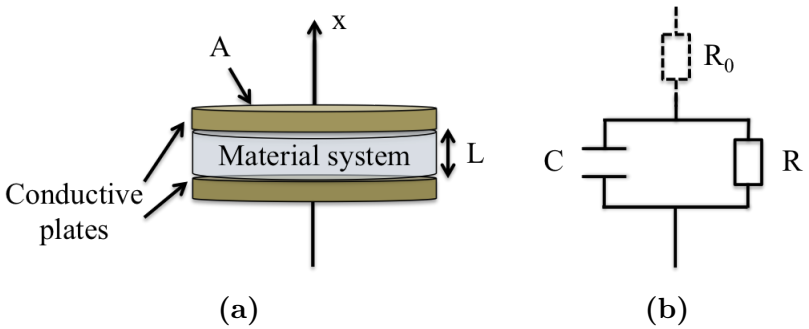

Figure 2.1: (a) Material system mounted between two conductive plates forming a parallel plate capacitor and (b) the equivalent electric circuit (solid) consisting of a capacitance C in parallel with a resistance R (the dashed part of the circuit is an internal resistance of the measurement circuit).

For characterization of this system one is interested in the electric field, $E(x,t)$, and the conduction current density, $j(x,t)$, which are functions of time t and space x. However, only the integral quantities U (voltage) and I_{tot} (total current) can be measured. Information on the spatial distribution is lost due to averaging

$$U = \int_0^L E \cdot dx \tag{2.1}$$

$$I_{tot} = \int j_{tot} \cdot dA. \tag{2.2}$$

The field strengths and the current densities presented later on are average values which have been calculated by dividing the absolute current and voltage by the sample area and the sample thickness, respectively.

$$\langle E \rangle = \frac{U}{L} \tag{2.3}$$

$$\langle j_{tot} \rangle = \frac{I_{tot}}{A} \tag{2.4}$$

For simplicity, the brackets will be skipped in the future. Furthermore, measurement errors of L and A, which need to be determined also experimentally, lead to errors in E and j_{tot}. The total current I_{tot} that is measured consist of a conduction current contribution and a displacement current contribution according to

$$I_{tot} = I + \dot{Q} = I + C\dot{U} + \dot{C}U. \tag{2.5}$$

Here, Q is the electrical charge and C the capacitance, which are related by $Q = CU$. From equation (2.5) one finds that even at constant voltage ($\dot{U} = 0$) temporal changes in C imply current contributions ($\dot{C}U$), which may lead to wrong conclusions. These changes in C can for example be caused by temporal changes in temperature or humidity.

Due to finite size effects and the influence of contacts the dielectric properties studied should be thought of as system properties rather than actual bulk properties.

2.1 Brief overview on linear dielectric spectroscopy

To understand nonlinear dielectric spectroscopy it is essential to first understand linear dielectric spectroscopy. The interest in dielectric properties and spectroscopy investigations can be traced back to the late nineteenth century and the science within this area may be considered as well established [3, 4, 5]. The basic idea of dielectric spectroscopy is to measure dielectric properties as a function of frequency

by letting a sample interact with a harmonically oscillating electric field. When applying a periodic voltage $U(t) = U_0 \cos(\omega t)$ with frequency $f = \omega/2\pi$ to a system (in the following we will use the term "frequency" for the angular frequency), the resulting current has in linear response the form:

$$I_{tot}(t) = I_1^{'} \cos(\omega t) + I_1^{''} \sin(\omega t) \tag{2.6}$$

with Fourier coefficients,

$$I_1^{'} = \frac{2}{T} \int_0^T \cos(\omega t) I(t)\ dt \tag{2.7}$$

$$I_1^{''} = \frac{2}{T} \int_0^T \sin(\omega t) I(t)\ dt. \tag{2.8}$$

Two important dielectric properties which are usually studied with linear dielectric spectroscopy are the electrical conductivity and the permittivity. The field strength and current density can equivalently be related by the following equations.

$$j = (\sigma^{'} + i\omega\epsilon_0\epsilon^{'})E \tag{2.9}$$

$$j = \sigma^* E \tag{2.10}$$

$$j = i\omega\epsilon_0\epsilon^* E \tag{2.11}$$

Here the prime symbol indicates the real part of the quantities (imaginary parts will be denoted with double prime symbols) and the asterisk indicates complex quantities. The conductivity and the permittivity are in general complex and frequency dependent ($\omega = 2\pi f$):

$$\sigma^*(\omega) = \sigma'(\omega) + i\sigma''(\omega) \tag{2.12}$$

$$\epsilon^*(\omega) = \epsilon'(\omega) - i\epsilon''(\omega) \tag{2.13}$$

The conductivity measures a material's ability to conduct a current. For DC (i.e. $\omega = 0$), σ is real and by definition equals the ratio between the conduction current density, j, and the applied field:

$$\sigma = \frac{j}{E} \tag{2.14}$$

The permittivity is related to the phenomena that a dielectric material becomes polarized in response to an applied electric field and thereby reduces the net electric field. In the case of a linear and isotropic medium the permittivity relates the displacement field and the electrical field as $D = \epsilon E$. The real part of the permittivity ϵ', also referred to as the dielectric constant, is related to the energy stored in the material due to the response to the external field. The imaginary part ϵ'' is related to the loss of energy within the medium. The Kramer-Kronig relations relates ϵ' and ϵ'' but will not be discussed here, for further information see [12].

The real and imaginary parts of the conductivity and the permittivity are related to the amplitudes (or rms-values) $I^{'}$, $I^{''}$ and U_0 by:

$$\sigma^{'} = \frac{I^{'}}{U_0} \cdot \frac{L}{A} \tag{2.15}$$

$$\sigma^{''} = -\frac{I^{''}}{U_0} \cdot \frac{L}{A} \tag{2.16}$$

$$\epsilon^{'} = -\frac{I^{''}}{U_0} \cdot \frac{L}{\omega \epsilon_0 A} \tag{2.17}$$

$$\epsilon'' = \frac{I^{'}}{U_0} \cdot \frac{L}{\omega \epsilon_0 A}. \tag{2.18}$$

In the manual of the Novocontrol IS equipment that has been used [13], the relations between these quantities are defined in a slightly different way, which changes the sign of the imaginary part of the conductivity. Throughout this report we will consistently use the definitions above.

The complex conductivity and the complex permittivity contain the same information and it is a matter of taste which representation to use. In this thesis mainly the real part of the conductivity together with the real part of the permittivity will be considered.

Another quantity often discussed for AC insulation material is the dissipation factor, or loss angle, $\tan(\delta)$ which is defined as the ratio between the imaginary and real part of the permittivity and expresses the loss-rate of energy,

$$\tan(\delta) = \frac{\epsilon''}{\epsilon'}. \tag{2.19}$$

For applications, the value of $\tan(\delta)$ at the utility frequency (50 Hz in Europe or 60 Hz in U.S.) is most relevant.

Furthermore, in applications the power loss density p,

$$p = \frac{1}{T}\int_0^T jE\ dt \tag{2.20}$$

is an important quantity, because it couples to the heat balance equation which describes the thermal behaviour.

With the current density j corresponding to the current in equation (2.6) and the applied field $E = E_0\cos(\omega t)$, the power loss density equals $\frac{1}{2}j_1^{'}E_0$. If $j_1^{'} = \sigma^{'}E_0$, the power loss density can be expressed (in terms of the quantities discussed above) as

$$p = \frac{1}{2}\sigma^{'}E_0^2 = \frac{1}{2}\omega\epsilon_0\epsilon^{'}\tan(\delta)E_0^2. \tag{2.21}$$

2.1.1 Example: Drude-Debye model

In this section an example is provided where the resulting current flowing through a linear dielectric material is calculated when an electric field is applied. The total current density, j_{tot}, is a sum of the conduction current density and the displacement current density,

$$j_{tot} = j + \dot{D} \tag{2.22}$$

where in this example j is the conduction current

$$j = \sigma E. \tag{2.23}$$

This term is related to the movement of "free" charge carriers through the material. In this example the conductivity σ is assumed to be constant ($\sigma = \sigma_0$) in accordance with the Drude conduction model, where the conductivity is due to carriers with constant density n and mobility μ:

$$\sigma = e\sum_i \mu_i n_i \tag{2.24}$$

Here i denotes the different carrier species.

The displacement current density $\dot{D}$ corresponds to the rate of change of the electric displacement field,

$$D = \epsilon_0\epsilon_\infty E + P \tag{2.25}$$

where ϵ_0 is the permittivity of vacuum and ϵ_∞ is the high-frequency ("optical") dielectric constant. From equation (2.22) and (2.25) the total current density equals

$$j_{tot} = \sigma E + \epsilon_0 \epsilon_\infty \dot{E} + \dot{P}. \tag{2.26}$$

The second term is due to the quasi instantaneous displacement of the fast dipoles and the permittivity of free space. The third term is due to changes in the polarization, e.g. due to slow displacements of polar polymer chains, and contributes to the total current. Another alternative can be trapped charge carriers, which do not freely move in the material as the conducting carriers do. Since this work concerns characterization of DC insulation systems, where current contributions due to temporal changes vanishes, primarily the conduction current will be considered. Nevertheless, this example is discussed for completeness.

The polarization P is given by the Debye dipole relaxation model,

$$\tau_p \dot{P} = \epsilon_0 \chi E - P \tag{2.27}$$

where τ_p is a characteristic relaxation time and χ is the electric susceptibility, and both τ_p and χ are constant. We now assume the applied field $E = E_0 \cos(\omega t)$ and make the ansatz for the solution of the differential equation

$$P = A\cos(\omega t) + B\sin(\omega t), \tag{2.28}$$

which leads to the following amplitudes

$$\begin{cases} A = \frac{\epsilon_0 \chi E_0}{1+(\omega\tau_p)^2} \\ \\ B = \frac{\omega\tau_p \epsilon_0 \chi E_0}{1+(\omega\tau_p)^2}. \end{cases} \tag{2.29}$$

This gives the total current density,

$$j_{tot} = \left[\sigma_0 E_0 + \frac{\tau_p \omega^2 \epsilon_0 \chi E_0}{1+(\omega\tau_p)^2}\right]\cos(\omega t) - \left[\epsilon_0 \epsilon_\infty \omega E_0 + \frac{\omega \epsilon_0 \chi E_0}{1+(\omega\tau_p)^2}\right]\sin(\omega t). \tag{2.30}$$

Furthermore, $j_{tot} = (\sigma^{'} + i\omega\epsilon_0\epsilon^{'})E^*$ where the asterisk denotes that the complex electric field is considered ($E^* = \frac{1}{2}E_0 e^{i\omega t}$). Since it was assumed that $E = E_0\cos(\omega t)$, the total current density is found by adding $(\sigma^{'} + i\omega\epsilon_0\epsilon^{'})E^*$ and its complex conjugate resulting in

$$j_{tot} = \sigma^{'} E_0 \cos(\omega t) - \omega\epsilon_0\epsilon^{'} E_0 \sin(\omega t). \tag{2.31}$$

From comparison of equation (2.30) and (2.31) the real parts of the conductivity and the permittivity can be identified.

$$\begin{cases} \sigma^{'}(\omega) = \sigma_0 + \frac{\tau_p \omega^2 \epsilon_0 \chi}{1+(\omega\tau_p)^2} \\ \epsilon^{'}(\omega) = \epsilon_\infty + \frac{\chi}{1+(\omega\tau_p)^2} \end{cases} \tag{2.32}$$

Figure 2.2 shows an example of how these quantities behave with frequency for a certain choice of parameters. As can be seen, the real conductivity and the real permittivity reach plateau values in the limits $\omega \to 0$ and $\omega \to \infty$. The value $\sigma^{'}(\omega \to 0)$ is often referred to as the DC conductivity and the value $\epsilon^{'}(\omega \to \infty)$ is called the high-frequency ("optical") dielectric constant.

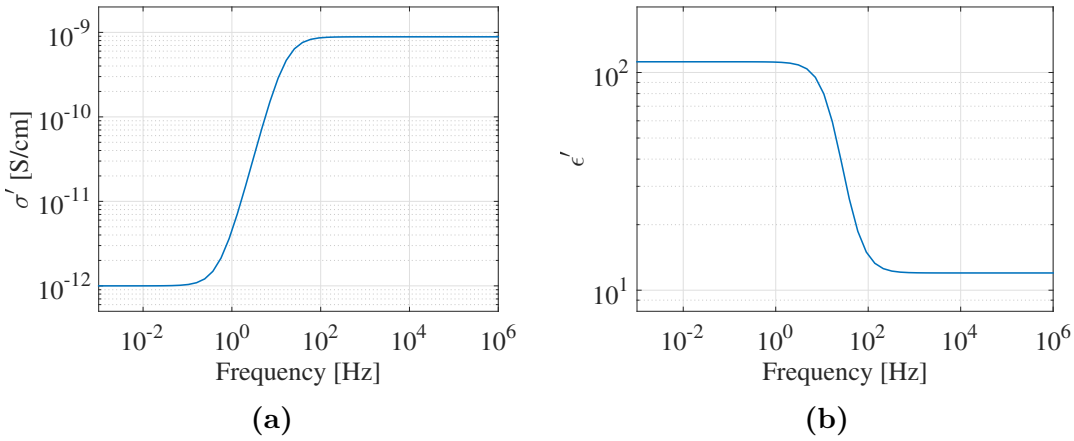

Figure 2.2: The frequency behaviour of the real electrical conductivity ($\sigma^{'}$) and the real permittivity ($\epsilon^{'}$) for a specific set of parameters.

In equation (2.32) one can see that $\epsilon^{'}$ is a function of $\omega\tau_p$. If a linear response function (like $\epsilon^{'}$ or $\sigma^{'}$) has this property, it follows that a change of τ_p (e.g. via changing the temperature) results in a shift of the curve on the logarithmic frequency axis. This means that plots done for different τ_p values will collapse to a single curve if appropriately shifted (a so-called master curve). However, this requires the relevance of a single characteristic time, which is in general not the case. An example is even $\sigma^{'}$ in equation (2.32), because there are two relevant time scales (τ_p and ϵ/σ).

2.2 Nonlinearities and superharmonics

In this thesis nonlinear behaviour generally refers to a nonlinear current response to an applied electric field. The presence of nonlinearities implies the existence of higher harmonics, also called superharmonics, i.e. current amplitudes at integer multiples of the fundamental frequency of the applied voltage. The stronger the nonlinearty is the more important it becomes to take the superharmonics into account since a greater part of the total current then is contained in the higher harmonics. Figure 2.3 shows an illustrative example of a linear (to the left) and a nonlinear (to the right) current-voltage dependence. In the same figure the corresponding current

response in time domain to an applied field $E = E_0 \cos(\omega t)$ is shown, as well as the corresponding conduction current contributions for different harmonics. Here all the harmonic contributions are normalized to the current amplitude of the fundamental frequency. In the linear case all superharmonics vanish, while in the nonlinear case they constitute a significant part of the total current.

A general nonlinear current response $I(t)$ to a periodic voltage with fundamental frequency $f = \omega/2\pi$ can be written in the form of a Fourier series,

$$I(t) = I_0 + \sum_{k=1}^{\infty} \{I_k^{'} \cos(k\omega t) + I_k^{''} \sin(k\omega t)\} \tag{2.33}$$

where I_0 is a DC offset component and the index k indicates the order of the harmonic. The frequency component at k times the fundamental frequency is called the kth harmonic. The Fourier coefficients $I_k^{'}$ and $I_k^{''}$ are

$$I_k^{'} = \frac{2}{T} \int_0^T \cos(k\omega t) I(t)\ dt \tag{2.34}$$

$$I_k^{''} = \frac{2}{T} \int_0^T \sin(k\omega t) I(t)\ dt. \tag{2.35}$$

Assuming that the applied field is of the form $E = E_0 \cos(\omega t)$, the coefficients $I_k^{'}$ may contribute to the conduction current. This is because for a steady state ($\omega = 0$), the total DC conduction current is given by,

$$I = \sum_{k=0}^{\infty} I_k^{'}. \tag{2.36}$$

Note that the amplitudes $I_k^{'}(\omega)$ can also be zero for $\omega \to 0$.

In many simple cases, the $I_k^{''}$ terms belong to the displacement current. However, in general, free carriers and dipoles can contribute to both $I_k^{'}$ and $I_k^{''}$ if dynamic effects play a role, and the different contributions cannot be directly thought of as conduction currents and displacement currents respectively. This can be seen in the example with the Drude-Debye model that was provided in section 2.1.1, where the $I_1^{'}$ term not only depends on the free carriers but also on, for example, the relaxation time of the dipoles τ_p, see equation (2.30).

We now recall that the power loss density can be calculated from equation (2.20) and consider the current density corresponding to the current in equation (2.33). When calculating the power loss density for the applied field $E_0 \cos(\omega t)$ all terms vanish except for the one containing $I_1^{'}$, or equivalent $j_1^{'}$, and the result becomes $\frac{1}{2} j_1^{'} E_0$.

When dealing with Fourier series, like the one in equation (2.33), there are symmetries that are helpful to keep in mind. One important symmetry is the time reversal

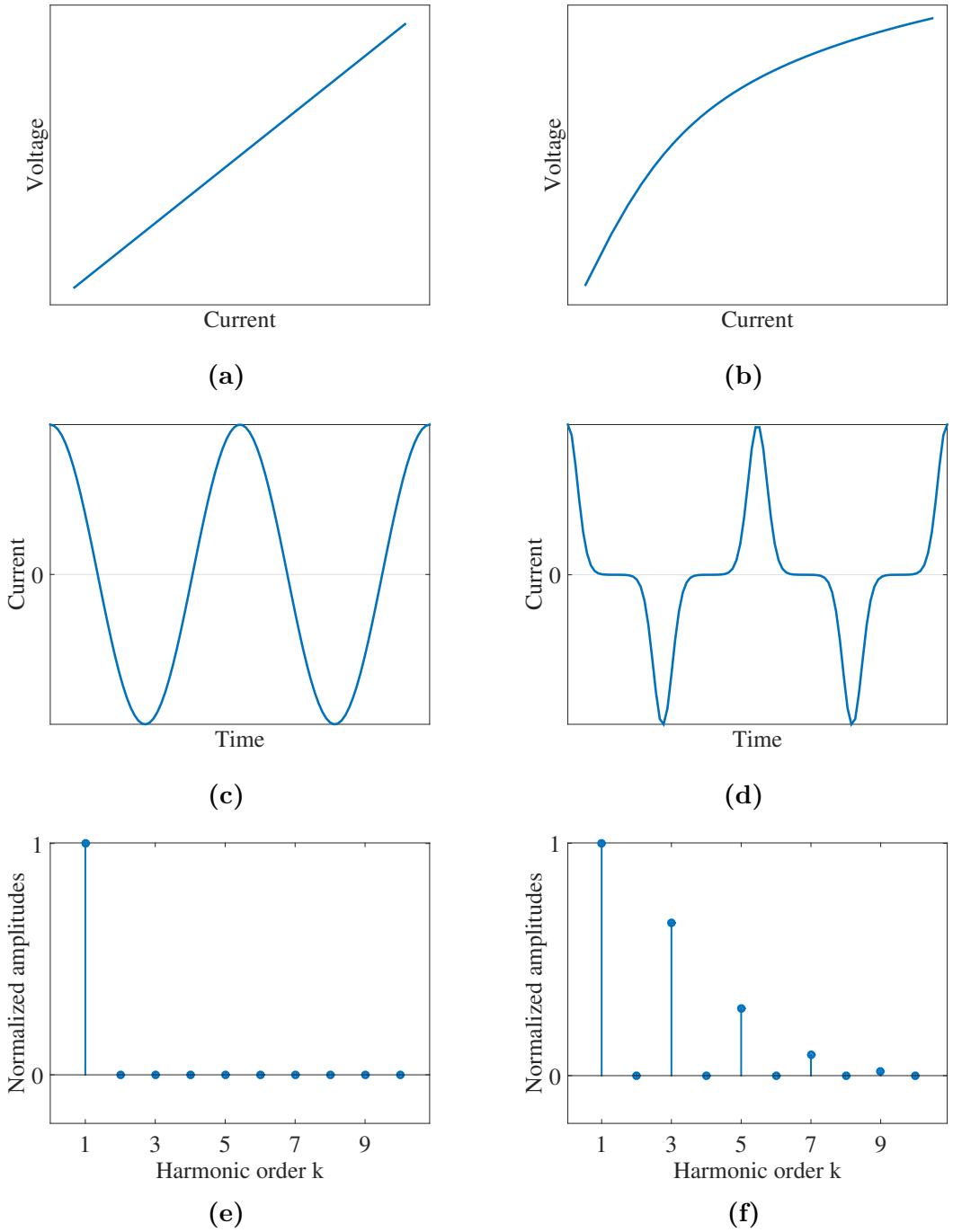

Figure 2.3: Example of a linear and nonlinear current-voltage characteristics (a respectively b), the corresponding current response in time domain (c respectively d) and the corresponding current contributions $I^{'}$ for different harmonics (e respectively f). The displacement current is not shown here, it would have an amplitude of the fundamental frequency (linear).

symmetry which states that since the field $E(t)$ remains invariant under $\omega \rightarrow -\omega$ (or equivalent $t \rightarrow -t$) the current $I(t)$ must not change either, $I_\omega(t) = I_{-\omega}(t)$ (or $I_\omega(t) = I_\omega(-t)$). Using this symmetry for the current in equation (2.33) one finds that $I_k^{'}(\omega) = I_k^{'}(-\omega)$ and $I_k^{''}(\omega) = -I_k^{''}(-\omega)$. For linear cases this means $\sigma^{'}(\omega) = \sigma^{'}(-\omega)$ and $\epsilon^{'}(\omega) = \epsilon^{'}(-\omega)$.

Another symmetry arises if the transformation $E_0 \rightarrow -E_0$ (or equivalently $\omega t \rightarrow \omega t + \pi$) leads to $I \rightarrow -I$, which is e.g. valid for odd current-voltage characteristics. This affects the even harmonics ($k = 2l$) in equation (2.33) since $\cos(2l\omega t + 2l\pi) = \cos(2l\omega t)$ and $\sin(2l\omega t + 2l\pi) = \sin(2l\omega t)$. Since this transformation does not change the direction of the current this only holds if $I_{2k}^{'} \equiv 0$ and $I_{2k}^{''} \equiv 0$. In practice this symmetry applies for samples where changing the direction of the field, or turning the sample, does not affect the results. Examples will be discussed later.

Materials or material systems with expected significant nonlinear response will in this thesis be divided into two main categories, namely materials with micro-interfaces and materials with macro-interfaces. This classification is based on which type of physics that determines the conduction in the system. Modelling of materials belonging to the micro-interface class is easier than material systems with macro-interfaces. This is because they are heterogeneous materials that can be described by average material quantities. Nonlinearities caused by macro-interfaces will be further discussed in two examples given in the end of this chapter.

In what follows, an alternative representation of electric nonlinear behaviour is introduced, which differs from the commonly seen DC characteristics (i.e. the steady-state current-field characteristics). With this description both nonlinearities and frequency dependencies are taken into account [14]. The time-periodic behaviour is studied in the form of hysteresis curves, where the current density or the displacement field is plotted against the electric field for a certain frequency. This type of representation in commonly used for ferroelectric materials or in electrochemistry, where the plots are called "cyclic voltammogram", but has also been applied to field grading materials [15].

The shape of the curves can provide information about the electrical behaviour at high fields and at different frequencies. For example, for displacement-electric field (D-E) loops the widening (opening) of the curves is related to the losses present in the system (heat production). From IS measurements of higher harmonics the time dependent behaviour can be constructed, which makes this representation possible without additional measurements.

We consider an example where the displacement field is given by

$$D = \epsilon_0 E + P \tag{2.37}$$

with P defined by

$$\tau_p \dot{P} = \epsilon_0 \chi(E) E - P. \tag{2.38}$$

In this example we assume the characteristic time τ_p to be constant and the electric susceptibility χ to be field dependent, consisting of one constant term and one term proportional to E^2. The total current density is then given by

$$j_{tot} = \sigma(E)E + \dot{D} \tag{2.39}$$

where the conductivity is assumed to have a nonlinear field dependence. Figure 2.4 shows how the two types of hysteresis curves can look like for this example. Both curves indicate a nonlinear behaviour of the system, with losses present.

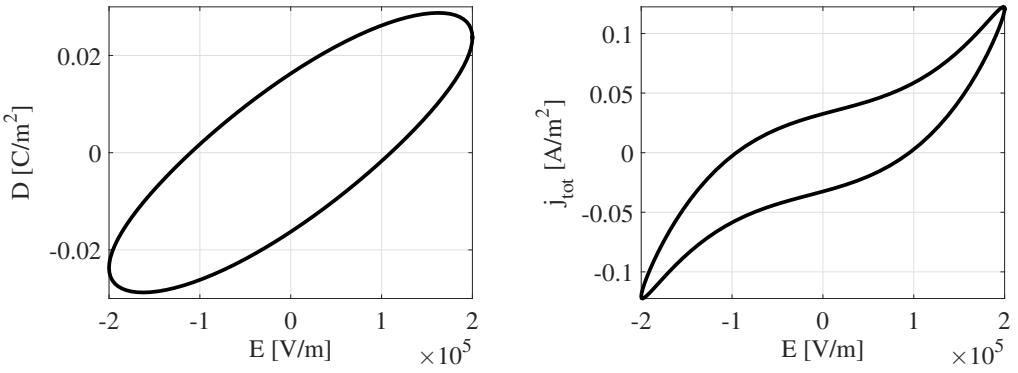

Figure 2.4: Example of two types of hysteresis curves: (a) displacement-electric field curve and (b) current density-electric field curve.

In figure 2.5 another example is provided of different current density-electric field curves. Here four different curves are shown, one with nonlinear behaviour of both the conduction current and displacement current, one with linear conduction current and nonlinear displacement, one with nonlinear conduction and linear displacement current and one with linear behaviour of both the conduction current and displacement current. Note that the power density is related to the frequency and the area of the closed curve [14].

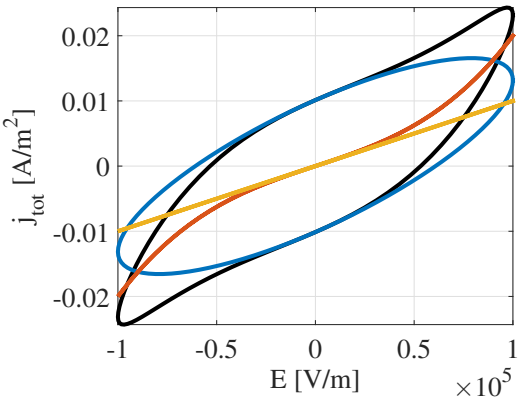

Figure 2.5: Example of different current density-electric field curves. Black: Nonlinear conduction and nonlinear displacement, blue: linear conduction and nonlinear displacement, red: nonlinear conduction and linear displacement, yellow: linear conduction and linear displacement.

In the following sections examples of different types of nonlinear behaviour are presented.

2.2.1 Example: Modelling of nonlinear I-V characteristics

Fitting experimental data to different conduction models can contribute to the understanding of the underlying physical processes that determines the conductivity of a material. Within the scope of this thesis, the material systems considered will not be modelled with the purpose of understanding details of the conduction mechanisms. Although, it will be emphasised how to use modelling as a part of a characterization process. In this section the general idea of how to fit experimental data from dielectric spectroscopy to existing conduction models is explained. We will here consider the simple case where the conduction current density, $j(E)$, is an odd, nonlinear function of the field strength:

$$j(E) = \sum_{n \ odd} a_n E^n. \tag{2.40}$$

Note that this example does not apply for all models, but demonstrates some simple cases. This type of current-field relation can, for example, physically be explained by a field dependent mobility. For a harmonic field $E = E_0 \cos(\omega t)$, the current density can be written as a function of time:

$$j(t) = \sum_{n \ odd} a_n E_0^n \ \cos^n(\omega t). \tag{2.41}$$

In accordance with equation (2.33), the current density can in this case be written in the form $j(t) = \sum_k j_k' \cos(k\omega t)$. The Fourier coefficients, j_k', are then given by the

following expression (from combining equation (2.41) and (2.34)).

$$j_k^{'} = \frac{2}{T}\int_0^T \sum_{n\ odd} a_n E_0^n\ \cos(k\omega t)\cos^n(\omega t)\ dt \tag{2.42}$$

The coefficients $j_k^{'}$ contain equivalent information as the data given by a dielectric spectroscopy measurement of higher harmonics. For simplicity, we introduce the coefficients g_k^n:

$$g_k^n = \frac{2}{T}\int_0^T \cos(k\omega t)\cos^n(\omega t)\ dt. \tag{2.43}$$

Hence, equation (2.42) can be written as

$$j_k^{'} = \sum_{n\ odd} g_k^n\ a_n E_0^n. \tag{2.44}$$

We continue now by calculating the coefficients g_k^n by first using that $T = 2\pi/\omega$ and then making the variable change $z = \omega t$.

$$g_k^n = \frac{\omega}{\pi}\int_0^{\frac{2\pi}{\omega}} \cos(k\omega t)\cos^n(\omega t)\ dt = \frac{1}{\pi}\int_0^{2\pi} \cos(kz)\cos^n(z)\ dz \tag{2.45}$$

Moreover, the cosine parts can be expressed in terms of exponential functions.

$$g_k^n = \frac{1}{\pi}\int_0^{2\pi} \frac{1}{2}(e^{ikz} + e^{-ikz})\frac{1}{2^n}(e^{iz} + e^{-iz})^n\ dz \tag{2.46}$$

Next, the following binomial formula was used,

$$(x+y)^n = \sum_{l=0}^{n} \binom{n}{l} x^{n-l}y^l \tag{2.47}$$

resulting in,

$$g_k^n = \frac{1}{2\pi}\int_0^{2\pi} \frac{1}{2^n}\sum_{l=0}^{n}\binom{n}{l}(e^{i(2l+k-n)z} + e^{-i(2l-k-n)z})\ dz. \tag{2.48}$$

Since $\int_0^{2\pi} e^{i\alpha z}dz = 0$ for all nonzero integers α, the only remaining terms will be the ones that fulfil $2l = n \pm k$. Therefore, $g_{k=even}^n \equiv 0$ and the g_k^n for odd k values can be expressed as

$$g_k^n = \frac{1}{2^n}\left[\binom{n}{\frac{1}{2}(n-k)} + \binom{n}{\frac{1}{2}(n+k)}\right]. \tag{2.49}$$

Because $n - \frac{1}{2}(n-k) = \frac{1}{2}(n+k)$, the two terms in this sum are equal. The final result of the coefficients g_k^n is

$$g_k^n = \frac{1}{2^{n-1}} \binom{n}{\frac{1}{2}(n+k)} \quad \text{for} \quad k \leq n. \tag{2.50}$$

From this result the coefficients $j_k^{'}$ can be written as follows, in accordance with equation (2.44).

$$j_k^{'} = \sum_{n \ odd} \frac{1}{2^{n-1}} \binom{n}{\frac{1}{2}(n+k)} a_n E_0^n \tag{2.51}$$

If the coefficients $j_k^{'}$ are known from experimental data, a_n can be determined and that is equivalent to determining the actual model parameters. In table 2.1 the coefficients g_k^n are given for $n, k \leq 7$.

Table 2.1: Coefficients g_k^n for $n, k \leq 7$.

n \ k	1	3	5	7
1	1	-	-	-
3	$\frac{3}{4}$	$\frac{1}{4}$	-	-
5	$\frac{5}{8}$	$\frac{5}{16}$	$\frac{1}{16}$	-
7	$\frac{35}{64}$	$\frac{21}{64}$	$\frac{7}{64}$	$\frac{1}{64}$

As an example, if the current density can be described by $j(E) = \sigma_0 E^3$ and the field is given by $E = E_0 \cos(\omega t)$, the first and third harmonic will contribute to the total resulting current density. These contributions are given by $j_1^{'} = \frac{3}{4}\sigma_0 E_0^3$ and $j_3^{'} = \frac{1}{4}\sigma_0 E_0^3$ (all a_n are zero except a_3 which is equal to σ_0). Equation (2.36) then reads $j = j_1^{'} + j_3^{'} = \sigma_0 E_0^3$ which is obviously correct (the sum of all numbers in a row of table 2.1 equals one).

2.2.2 Example: Piecewise constant conductivity

This example is a simple description of field grading materials (see section 4.1), where the physics is based on interfaces between or inside particles that are filled in polymers. The conductivity is described by

$$\sigma(E) = \begin{cases} 0 & |E| < E_c \\ \sigma_0 & |E| \geq E_c \end{cases} \tag{2.52}$$

where σ_0 and E_c are constants. This means that the conductivity is zero for all field strengths smaller than E_c and has a constant value for field strengths larger than E_c. The field dependence of the conductivity implies a nonlinear field dependence of the current density, which gives rise to superharmonics. Considering the conductivity in equation (2.52) and the harmonic field $E = E_0 \cos(\omega t)$, with $E_0 > E_c$, results in the conduction current density:

$$j(E) = \begin{cases} \sigma_0 E_0 \cos(\omega t) & 0 \leq t \leq t_c \\ 0 & t_c \leq t \leq \frac{\pi}{\omega} - t_c \end{cases} \tag{2.53}$$

Here, t_c is defined as the first time the field strength is equal to E_c, i.e. $E_0 \cos(\omega t_c) = E_c$ (or $\omega t_c = \arccos(\frac{E_c}{E_0})$). In equation (2.53) the current density is only described in the first two intervals that arise from the discontinuity of the conductivity. The behaviour of the current density as a function of time, $j(t)$, can be seen for a whole period, $T = \frac{2\pi}{\omega}$, in figure 2.6.

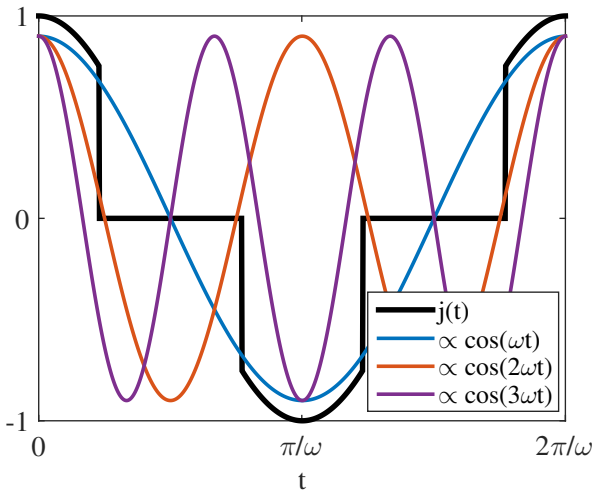

Figure 2.6: Current density as a function of time for the case with a piecewise constant conductivity, shown together with cosine functions of different frequencies (corresponding to different multiples of the fundamental frequency).

The displacement current density is not considered here. The harmonic current components $j_k^{'}$ are calculated (in accordance with equation (2.34) in section 2.1) from

$$j_k^{'} = \frac{\omega}{\pi} \int_0^{2\pi/\omega} j(t) \cos(k\omega t)\ dt \tag{2.54}$$

by summing up integrals over the nonzero intervals, i.e. the different intervals where $j(t)$ is nonzero. In figure 2.6 the cosine functions which appear in the integral are shown for $k = 1, 2, 3$ together with $j(t)$ for visualization. The calculations can be be done analytically (see appendix A for full calculations of $j_1^{'}$ and $j_3^{'}$) and $j_k^{'}$ is given by

$$j_k' = \frac{\sigma_0 E_0}{\pi}\left[\frac{2}{k-1}\sin\left((k-1)\arccos(\frac{E_c}{E_0})\right) + \frac{2}{k+1}\sin\left((k+1)\arccos(\frac{E_c}{E_0})\right)\right] \quad \forall \text{ odd k} \geq 1. \tag{2.55}$$

Note that for $k = 1$ the limit $k \to 1$ with $\lim_{\epsilon\to 0}\frac{\sin(\epsilon x)}{\epsilon} = x$ holds. Since the current-voltage characteristics is symmetric around the origin, all amplitudes of even superharmonics vanish.

In figure 2.7 the current contributions j_k' are shown for different harmonic orders for a certain choice of E_0, E_c and σ_0. Note that all even harmonics are zero while the odd harmonics take on both positive and negative values. The significant contributions of the superharmonics are reasonable because of the strongly nonlinear nature of this problem.

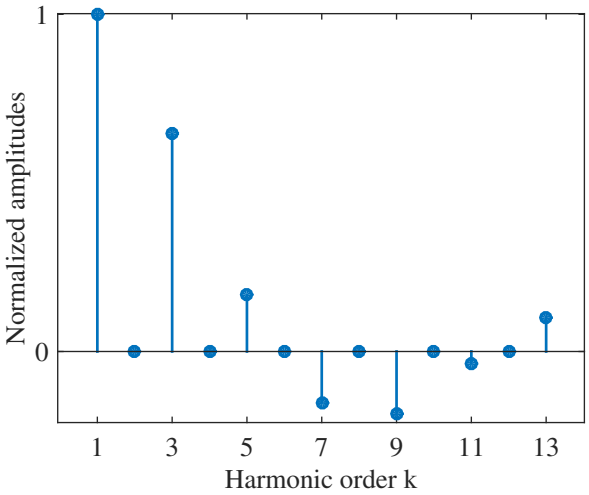

Figure 2.7: Current contributions j_k' for different harmonic orders. The amplitudes are normalized with respect to the fundamental frequency, corresponding to $k = 1$.

From the superharmonics the current-field relation can be reconstructed,

$$j(E) = \sum_{k=1}^{N} j_k' \tag{2.56}$$

where N is the highest harmonic considered. This was done for several different values of N, see figure 2.8. As can be seen, the curves converge towards the complete reconstruction (including all superharmonics) for increasing value of N.

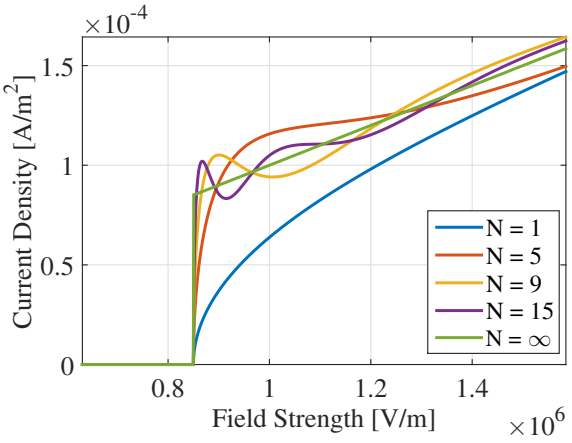

Figure 2.8: Current-field relation reconstructed from the current density contributions j_k' for different number of harmonics included.

2.2.3 Example: Schottky barrier

In this example a non-symmetric case of current-voltage characteristics is considered, namely a so called Schottky barrier,

$$I = I_0(e^{-\frac{eU}{kT}} - 1) \tag{2.57}$$

where I_0 is a constant, e the elementary charge, U the voltage, k Boltzmann's constant and T the temperature. The corresponding current-voltage voltage characteristic can be found in figure 2.9. In this case the current is not an odd function of the voltage which leads to nonzero even superharmonics, as will be shown. Schottky barriers appear at interfaces of materials with different carrier properties, like p-n semiconductor junctions.

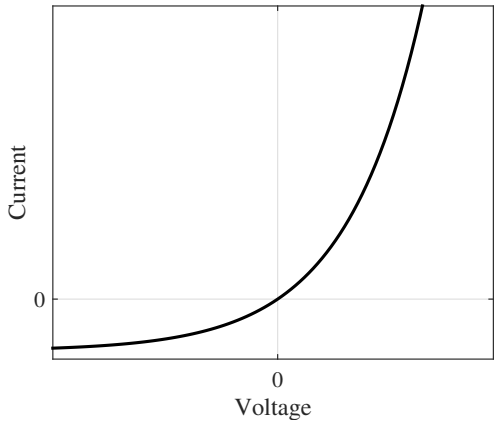

Figure 2.9: Current-voltage characteristics of the Schottky barrier.

Assuming a harmonic voltage $U = U_0 \cos(\omega t)$ and making a Taylor expansion of the exponential function gives

$$I(t) = \sum_{n=1}^{\infty} C_n \cos^n(\omega t) \qquad C_n = \left(-\frac{eU_0}{kT}\right)^n \frac{1}{n!} \tag{2.58}$$

With the use of equation (2.34) the first even superharmonic contribution to the conduction current $I_2^{'}$ can be calculated.

$$\begin{aligned} I_2^{'} &= \tfrac{2}{T}\int_0^T \cos(2\omega t) I(t)\, dt = \textstyle\sum_{n=1}^{\infty} C_n \, \tfrac{\omega}{\pi} \int_0^{2\pi/\omega} \cos(2\omega t)\cos^n(\omega t) dt \\ &= \tfrac{1}{2}C_2 + \tfrac{1}{2}C_4 + \tfrac{15}{32}C_6 + \ldots \neq 0 \end{aligned} \tag{2.59}$$

Figure 2.10 shows normalized current contributions for the five first harmonics for a certain choice of parameters. As can be seen, the even harmonics do not vanish in this non-symmetric example.

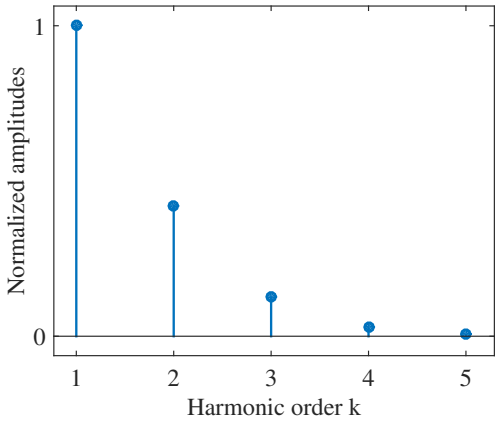

Figure 2.10: Current contributions $I_k^{'}$ for the five first harmonics. The amplitudes are normalized with respect to the fundamental frequency, corresponding to $k = 1$.

2.2.4 Example: Blocking contacts

In this section a theoretical model that illustrates the effect of blocking electrodes (a kind of macro-interfaces) is discussed [16]. Ion-blocking interfaces could for example be present in a system where two different materials are combined. If one of the materials contains a small amount of ions, these can be swept out of the bulk of this material and accumulate at the interface to the other material, causing a nonlinear behaviour.

Assume a quasi-neutral solid containing a single species of positive mobile carriers placed between a pair of blocking electrodes, see figure 2.11a. For a sufficiently high voltage the positive charge carriers will accumulate at the electrode with the lowest potential, forming a thin sheet of charges. This sheet of charge carriers will then

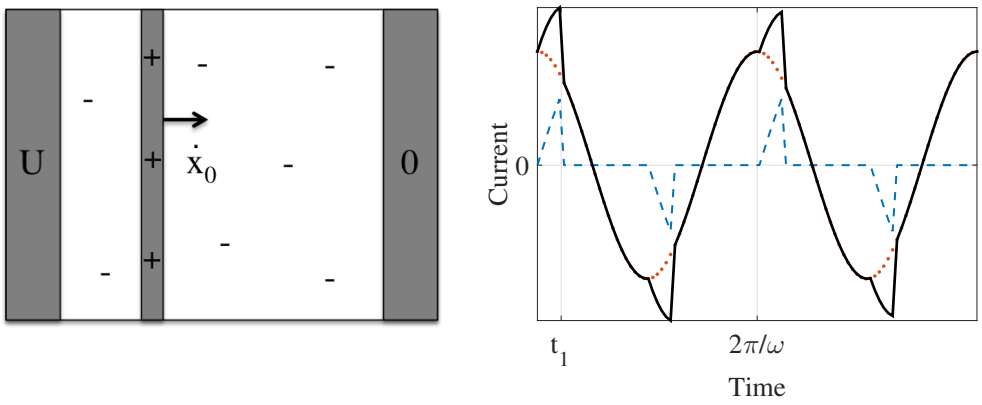

(a) **(b)**

Figure 2.11: (a) System with blocking electrodes and a moving charge sheet. (b) Current response: conduction current (red, dotted curve), displacement current (blue, dashed curve) and the total current (black, solid curve). Note that here, in contrast to the other examples, a sine voltage is applied and not a cosine voltage.

remain there until the polarity of the applied voltage changes and the charge drifts to the counter electrode.

The charge density $\rho(x)$ is given by

$$\rho(x) = q(\delta(x - x_0(t)) - \frac{1}{L}) \tag{2.60}$$

where $x_0(t)$ is the location of the positive charge sheet, q is the total charge per area and the term q/L represents the negative immobile background charge density. Knowing the charge distribution, the Poisson equation for the electric potential field Φ can be solved.

$$\Phi'' = -\frac{\rho(x)}{\epsilon} \tag{2.61}$$

Here the boundary conditions $\Phi(0) = U$ and $\Phi(L) = 0$ are used together with continuity of the potential at x_0 and discontinuity of the field at x_0 given by $\Phi|_{x_{0+}} - \Phi|_{x_{0-}} = q/\epsilon$. Solving the Poisson equation results in the intuitive average field value $\bar{E} = U/L$, see appendix A for complete calculations. Assuming a constant mobility, the drift velocity of the charge sheet is given by

$$\dot{x_0} = \mu \frac{U}{L}. \tag{2.62}$$

We now apply the voltage $U(t) = U_0 \sin(\omega t)$ and assume that the sheet of positive charges starts to move from the left electrode at $t = 0$. The location of the sheet is then received by integration of equation (2.62).

$$x_0(t) = \frac{\mu U_0}{\omega L}(1 - \cos(\omega t)) \tag{2.63}$$

We now defined the time t_1 as the time until the charge sheet first reaches the right electrode, meaning $x_0(t_1) = L$.

$$t_1 = \frac{1}{\omega} \arccos\left(1 - \frac{\omega L^2}{\mu U_0}\right) \tag{2.64}$$

Moreover, the polarity changes at the time π/ω, which corresponds to half of a period. The total current density is then given by

$$j(t) = \begin{cases} \epsilon\omega\frac{U_0}{L}\cos(\omega t) + q\mu\frac{U_0}{L^2}\sin(\omega t) & 0 \leq t < t_1 \\ \epsilon\omega\frac{U_0}{L}\cos(\omega t) & t_1 \leq t < \pi/\omega \end{cases} \tag{2.65}$$

where both the conduction current ($j = -\rho\dot{x_0}$) and the displacement current are included. The conduction current, displacement current and the total current can also be seen in figure 2.11b as a function of time. Here it is obvious that the conduction current, and hence the total current, behaves nonlinear.

In figure 2.12 the different harmonic contributions can be seen for a specific case of parameters. Note that the full amplitude of the fundamental frequency is not displayed here. Moreover, the $I_1^{''}$ of the displacement current is not shown.

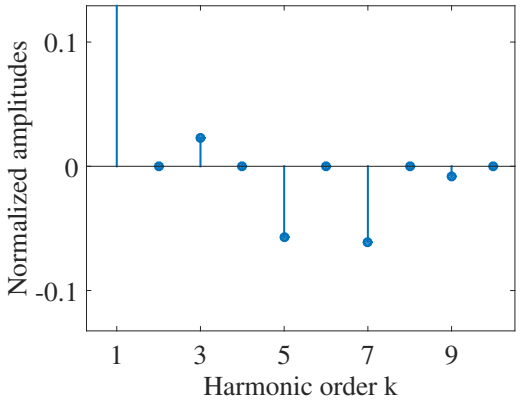

Figure 2.12: The current amplitudes $I_k^{'}$ normalized with respect to the fundamental frequency.

2.2.5 Space charge limited current

In this section another kind of macro-interfaces is considered, namely charge injecting contacts, and the principle of charge injection and space charge limited current is explained. Nonlinearity due to charge injecting contacts can occur in an insulator where the conduction is governed by charge injection from an ohmic electrode. The

theory of space charge limited current in solids between plane parallel electrodes was introduced already in 1940 by Mott and Gurney [17]. The phenomena can be observed for DC voltages and low frequency AC voltage, where the system reaches a quasi-steady state. In what follows, the space charge limited current in a perfect insulator is derived, the so called Mott-Gurney law.

Assume a plane plate sample (like the one in figure 2.1) with thickness L of a material that has no intrinsic conductivity, instead charges are injected from one of the electrodes. Moreover, the carrier mobility μ and the dielectric permittivity ϵ are assumed to be constant through the sample. This problem can then be defined by the following set of equations.

$$j = \rho v \tag{2.66}$$

$$\frac{dE}{dx} = \frac{\rho}{\epsilon} \tag{2.67}$$

$$U = \int_0^L E \cdot dx \tag{2.68}$$

Here, ρ is the space charge density and v the charge drift velocity. It is further assumed that the drift velocity is monotonically increasing with the electric field, i.e. $v = \mu E$. Inserting this in equation (2.66) gives

$$j = \rho \mu E. \tag{2.69}$$

Combining this with equation (2.67) we get

$$j = \epsilon \mu E \frac{dE}{dx} = \frac{1}{2} \epsilon \mu \frac{d(E^2)}{dx}. \tag{2.70}$$

Integrating equation (2.70) and assuming that the electric field is zero at the charge injecting electrode, i.e. $E(0) = 0$ (a so called ohmic electrode), results in

$$E(x) = \sqrt{\frac{2j}{\epsilon \mu}} x. \tag{2.71}$$

The electric potential across the sample can then be determined by inserting equation (2.71) in equation (2.68).

$$U = \frac{2}{3} \sqrt{\frac{2j}{\epsilon \mu}} L^{3/2} \tag{2.72}$$

By squaring and solving for the current density j, the well known Mott-Gurney law is obtained.

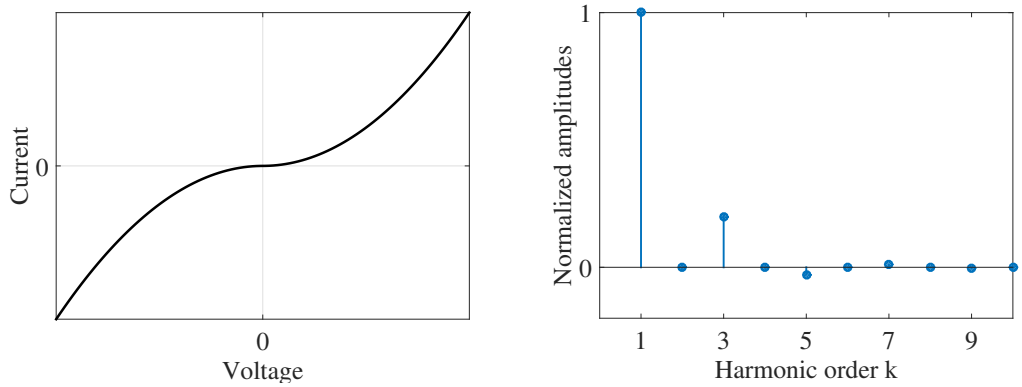

Figure 2.13: (a) Current-voltage relation in case of space charge limited current and (b) the corresponding harmonic contributions.

$$j = \frac{9}{8}\epsilon\mu\frac{|U|U}{L^3} \tag{2.73}$$

This current-voltage relation and the corresponding harmonic contributions for an applied voltage $U = U_0\cos(\omega t)$ can be seen in figure 2.13. Since the voltage dependence in equation (2.73) seems to be quadratic one could make the mistake to think that the second harmonic would contribute to the total current. However, this is not the case since the current is still an odd function of the voltage (note the difference between $|U|U$ and U^2).

Note that the quasi-steady state assumption means that the injection transient is fast compared to the frequency, i.e. $\omega\tau_{tof} \ll 1$, with the time of flight [18]

$$\tau_{tof} \cong \frac{L}{v} = \frac{L^2}{\mu U}. \tag{2.74}$$

This is the same as saying that the displacement current is negligible.

2.3 Dielectric spectroscopy and differential conductivity

In this section the principle of a IS measurement with AC voltage superimposed to a DC voltage will be described. This method provides information about the differential conductivity and will be used in this work to determine the current-field characteristics. In this type of measurements the applied voltage is a sum of a DC voltage and an AC voltage, resulting in a field of the form $E = E_0 + E_1\cos(\omega t)$. Here E_0 is a DC component and E_1 is the amplitude of the AC component, normally

$E_1 \ll E_0$. An illustration of how the applied field oscillates around a certain DC offset can be seen in figure 2.14.

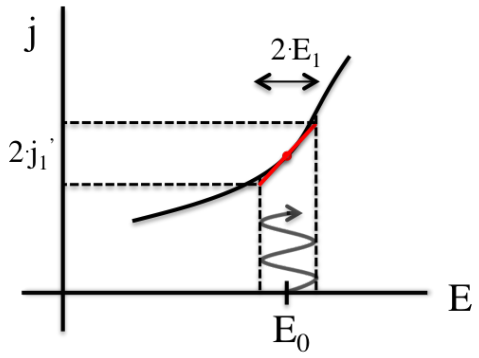

Figure 2.14: Illustration of the working principle of an IS measurement with applied AC voltage superimposed to a DC voltage, resulting in a field of the form $E = E_0 + E_1 \cos(\omega t)$. The field will oscillate around E_0, within the dashed lines, along the steady-state current-voltage characteristics (black, solid curve).

Due to the superimposed DC field these measurements can be done in the non-linear region and it is possible to probe material properties along the steady-state current-field characteristics. Therefore, this technique provides an additional way to characterize the response at high fields. We now define the differential conductivity and the differential permittivity:

$$\sigma_D = \frac{dj(E)}{dE} \tag{2.75}$$

$$\epsilon_D = \frac{1}{\epsilon_0}\frac{dD(E)}{dE}. \tag{2.76}$$

The differential conductivity is defined as the slope of the current-field characteristics at a certain field value. Analogously, the differential permittivity is proportional to the slope of the curve of the displacement field as a function of the electric field. Note that this definition is done for the limit $\omega \to 0$. This restriction can be relaxed but that goes beyond the purpose of this work. Although measurements are performed at finite frequency ω, we are mainly interested in the limit $\omega \to 0$:

$$\sigma_D = \sigma^{'}(E, \omega \to 0) \tag{2.77}$$

$$\epsilon_D = \epsilon^{'}(E, \omega \to 0) \tag{2.78}$$

where the prime symbol indicates measured (real) quantities.

By making several measurements with different DC fields the differential properties can be determined as functions of the electric field. From these functions the conduction current and displacement field can be found by integration:

$$j(E) = \int_0^E \sigma_D(\hat{E})\, d\hat{E} \tag{2.79}$$

$$D(E) = \epsilon_0 \int_0^E \epsilon_D(\hat{E})\, d\hat{E}. \tag{2.80}$$

For illustration we consider the following example, which shows how the conduction current and the displacement field can be constructed from the differential conductivity and the differential permittivity. Assume that $\sigma^{'}(E, \omega \to 0)$ and $\epsilon^{'}(E, \omega \to 0)$ can be fitted by

$$\sigma_D = \sigma_0(1 + 3c_1E^2) \tag{2.81}$$

$$\epsilon_D = k(1 + 3c_2E^2) \tag{2.82}$$

where σ_0, c_1, k and c_2 are constants. Using these expressions together with equation (2.79) and (2.80), the conduction current and displacement field can be determined:

$$J(E) = \sigma_0(1 + c_1E^2)E \tag{2.83}$$

$$D(E) = \epsilon_0 k(1 + c_2E^2)E \tag{2.84}$$

The results are shown for a certain choice of parameters σ_0, c_1, k and c_2 in figure 2.15. This method will later be used to reconstruct the I-V characteristics.

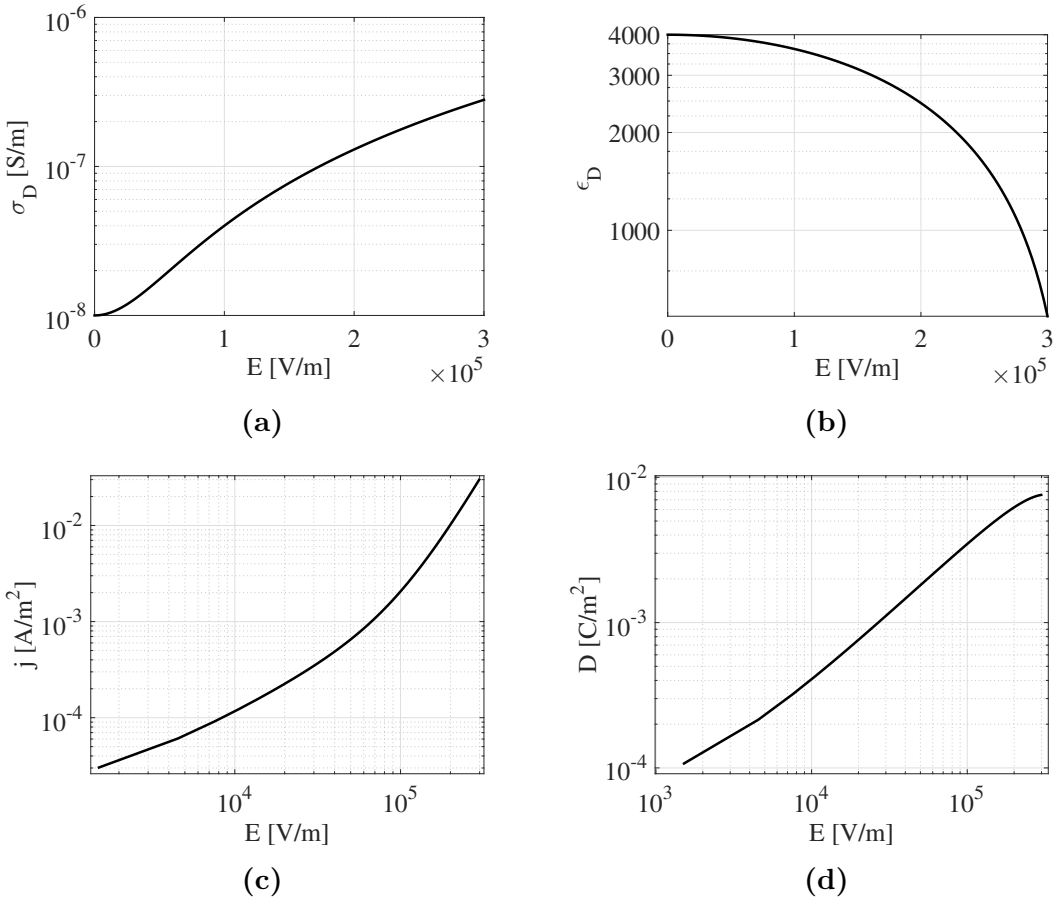

Figure 2.15: Example of how the conduction current and the displacement field can be constructed from (a) the differential conductivity and (b) the differential permittivity. Results are shown in (c) respectively (d).

3

Equipment and experiments

In this chapter different experimental equipment are described. Results from IS measurements are compared to results from two other setups, in this report referred to as IV-setup 1 and IV-setup 2, in order to check consistency of the methods and validate the nonlinear IS approach in praxis. All experiments were performed at ABB Corporate Research in Baden-Dättwil, by the author herself and by Roman Kochetov (ABB).

3.1 Impedance spectroscopy

The IS experiments were performed with a dielectric spectroscopy equipment provided by Novocontrol Technologies [19]. The working principle of a measurement is shown in figure 3.1.

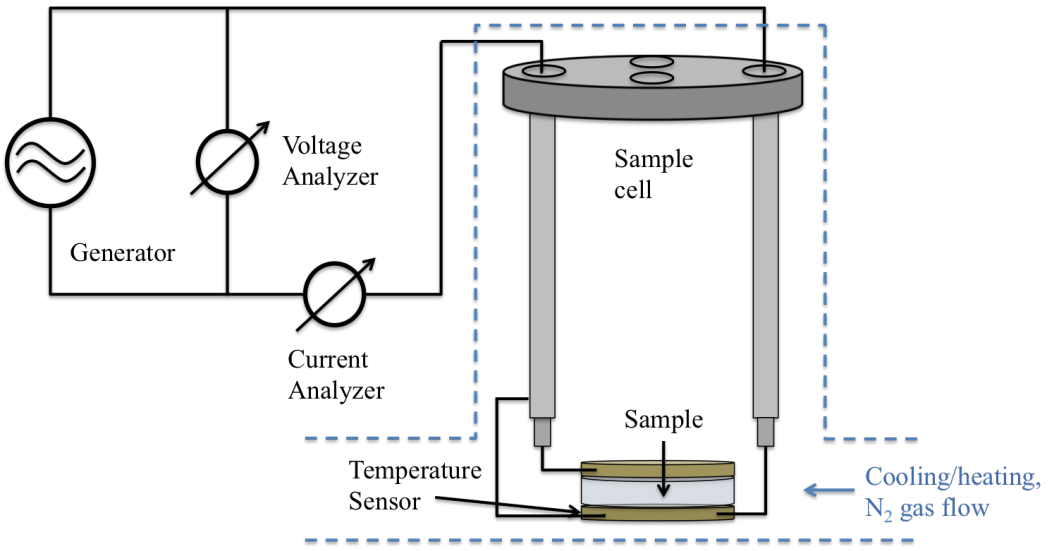

Figure 3.1: Principle of IS measurements.

The setup consists of:

- A frequency response analyzer (Alpha Analyzer), with a sine wave and DC-bias generator and two AC voltage input channels [20]. Each input channel

measures the AC voltage amplitude of an applied sine wave. Additionally the phase shift between the input waves is detected.

- A HV interface (HVB4000) enabling investigations at high AC voltages up to $U_{rms} = 1414\,V$ corresponding to amplitude peaks of 2 kV [21]. This interface also allows measurements of higher harmonics and measurements with applied AC voltage superimposed to DC voltage.
- A temperature controller (Quatro Cryosystem).
- Two different sample cells, one used for low voltage measurements and one for high voltage measurements. The sample capacitor is mounted between the upper and lower electrodes of the sample cell.
- A vaccum-isolated cryostat. The sample cell is placed inside the cryostat during measurements.
- A liquid nitrogen Dewar vessel.
- The software WinDETA, for control and evaluation of measurements [13].

Before starting any measurements the sample thickness was measured with the thickness gauge LE 1000-2, operated with the software ProWedge. It is important that these measurements are done accurately and that the sample thickness is homogeneous since uncertainties in the thickness are directly reflected in the results (see equation (2.15)-(2.18)) [22]. The sample was thereafter placed between external gold plated cylindrical electrodes. The sample capacitor was then mounted between the (fixed) upper and lower electrodes of the sample cell, which was then placed in the cryostat. The temperature of the system could be controlled between -160 °C − 400 °C.

To assure good contact between the sample and the external electrodes all non-elastic samples were evaporated with Cr and Au on both sides. Cr was used to improve the adhesion of Au with the sample. If the contact is bad and only parts of the sample are in contact with the external electrodes the contact area cannot be determined correctly, which leads to errors.

Three different types of measurements were performed with the IS setup:

1. **Small signal IS**: Linear response measurements in a wide frequency range ($10^{-4} - 10^{6}$ Hz) at low AC voltage ($U_{rms} = 1\,V$).
2. **High-Voltage IS**: Measurements of higher harmonics, up to the fifth harmonic or higher. These measurements were performed at rather high AC voltage amplitudes (up to $U_{rms} = 1414\,V$) for frequencies 1 mHz - 1 Hz.
3. **Superimposed DC-AC IS**: Measurements of the linear response to an AC voltage with superimposed DC voltage.

All IS measurements were fully automated and controlled by the WinDETA software [13]. When setting up a measurement up to four free variables can be chosen. Within this thesis work the following variable parameters were used (in different

combinations): frequency, temperature, AC voltage, harmonics and DC voltage. For each variable parameter chosen, value lists of desired data points were defined. After each measurement the data was saved in ASCII files and analyzed with MATLAB.

From the high-voltage IS measurements the output data consists of voltage and current amplitudes for each harmonic considered. The output data is normalized in such a way that the start time of an experiment $t = 0$ corresponds to a real positive cosine voltage (with zero phase angle). Throughout this report the current and its superharmonics will be defined according to equation (2.33), (2.34) and (2.35). However, Novocontrol uses a slightly different notation (which affects the sign of the sine coefficients) and therefore one needs to be careful when interpreting the output data from the equipment.

With the total current defined as in equation (2.33) the total current density equals

$$j_{tot} = \sum_{k=0}^{\infty} \{ j_k^{'} \cos(k\omega t) + j_k^{''} \sin(k\omega t) \} \tag{3.1}$$

where the amplitudes $j_k^{'}(E_0, \omega)$ and $j_k^{''}(E_0, \omega)$ depend on the field amplitude and the frequency. Due to symmetry reasons all amplitudes for even k vanish for the systems we consider (symmetric electrodes etc.) and the steady state conduction current $j(E)$ was calculated by letting $\omega \to 0$, resulting in

$$j(E) = \sum_{k \ odd}^{N} j_k^{'} \tag{3.2}$$

where N corresponds to the highest superharmonic measured.

The HV interface, which is used for measurement types 2 and 3 above, is internally connected to a current limiting resistor with $\mathrm{R}_0 = 750\,\mathrm{k}\Omega$ which protects the equipment. If the sample resistance is low, or comparable, to this resistance the voltage applied across the sample will be lower than the selected voltage. This internal resistance will only be considered if necessary. Necessity occurs if the voltage drop at R_0 is not negligible as compared to the applied voltage, $R_0 I_{tot} \sim U_0$, or if the sample impedance Z becomes so small that R_0/Z is no longer $\ll 1$.

3.2 IV-setup 1

This equipment from Novocontrol Technologies is made for thermally stimulated current (TSC) measurements and was used to check the consistency of steady state conduction current curves from high-voltage IS and superimposed AC-DC IS. The principle of an experiment is shown in figure 3.2 [23].

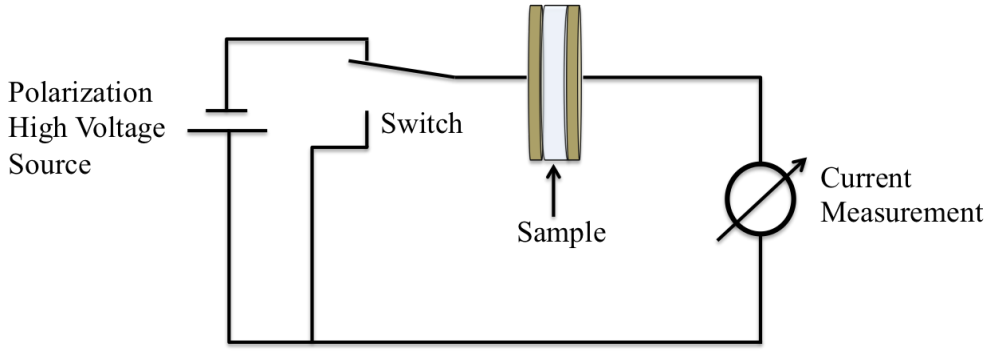

Figure 3.2: Principle of a TSC experiment.

With this setup several types of experiments can be performed. For our purpose measurements of isothermal polarization/depolarization currents were performed. A Keithley 6517B electrometer/high voltage source was used, which includes a built-in ± 1 kV voltage source and allows a broad current measurement range of 1 fA - 20 mA (noise level of 20 - 30 fA). The sample under investigation was placed between two electrodes to form a parallel plate capacitor. The sample capacitor was thereafter mounted in a sample cell, which was subsequently placed in a cryostat. A temperature control system was used that allows isothermal measurements (temperature stability of 0.01 °C) over a broad temperature range (-160 °C to 400 °C).

The principle of the experiment involves the following steps. First the temperature was set to a desirable value and the material was allowed to depolarize by applying a zero voltage to the electrodes (short circuit state). Then a polarization voltage was applied and the resulting current was measured over time. In theory, after some time the polarization current will settle down and a steady state current will be reached which corresponds to the conduction current. However, one has to be aware that a "DC-current" is always a point on a transient of a polarization current curve at a given time where equilibrium is often not yet established. This is because the equilibration times can be several days, or even weeks. Nevertheless, this setup allows for rather long waiting times ($> 10^4$ s), as compared to the next setup described.

3.3 IV-setup 2

This setup was developed at ABB for material characterization and was used within this work as an additional consistency check. A stepwise increasing DC voltage was applied to a sample and the resulting current was measured for each voltage value after a desired waiting time ($\sim$ 5 s). These measurements were performed at room temperature without temperature control. This lack of cooling needs to be taken into account when choosing the waiting time, in order to avoid heating of the sample. The setup allows the user to choose between two different voltage sources with maximum voltages of 3 kV respectively 20 kV. The stepwise increase of the voltage and the measurements were automatically controlled via a LabVIEW program.

This setup requires a different sample area than the IS setup and IV-setup 1. Hence, the very same samples were never tested with this setup as for the other two setups.

4

Material systems

An essential part of the work done within this thesis has been to find material systems which are insulating and appropriate for the investigation of nonlinearities. Materials or material systems with expected significant nonlinear response can, as previously explained, be divided into different categories depending on the reason of the nonlinear behaviour. Figure 4.1 shows a simple, but for our purpose sufficient, way to classify electrical nonlinear behaviour of insulation materials. First a separation is done between homogeneous materials (with intrinsic nonlinear properties, e.g. a field dependent mobility or a field dependent carrier density) and heterogeneous materials. Within this thesis focus has been on heterogeneous materials, that can be divided into two groups depending on whether their behaviour is governed by micro-interfaces (filled materials) or macro-interfaces. The latter include all sorts of interfaces between materials, e.g. between two insulators or at an electrode contact. Also the electrode contacts can be divided into sub-classes, like blocking electrodes and ohmic electrodes. For all cases the physical mechanism can have different origins, for instance direct electrical reasons or indirectly via thermal losses or temperature dependence.

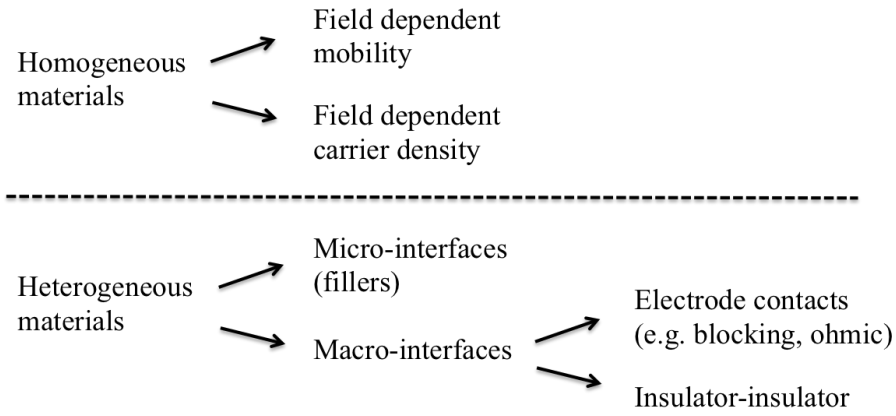

Figure 4.1: Classification of material systems with electric nonlinear behaviour.

In the following sections two classes of materials, namely materials with micro-interfaces and materials with macro-interfaces, are further explained and specific material systems that have been studied are introduced. Besides the material systems presented here a few other systems were also studied (e.g. silicone rubber

with different fillers, an insulating oil and series of polypropylene films) but without results useful for this thesis.

4.1 Materials with micro-interfaces: Nonlinear filled materials

This group of material systems are intrinsically nonlinear by their nature, like field grading materials and varistors. Electric field grading [14, 24, 25] is a technique that is used to avoid electric stress enhancements in high voltage devices by locally reducing the electric field. One way to control the field distribution is by using nonlinear field grading materials with appropriate current-field characteristics. A good field grading material is very resistive up to a certain field value where it drastically changes and becomes conductive. Desired nonlinear characteristics can be obtained with compounds of materials, such as an insulating polymer mixed with a semiconducting filler.

A varistor is a component with a nonlinear voltage dependent resistance. Varistors are used in surge arrestors. At low voltages the electrical resistance is high, but as the voltage is raised the resistance decreases. Two common filler particles are zinc oxide (ZnO) varistor micro-particles and silicon carbide (SiC). Using varistor particles as fillers in compounds is one way to achieve desired field grading properties. Figure 4.2 illustrates the interfaces appearing in two different polymer based materials, one filled with SiC particles and one filled with ZnO micro-varistor particles. The conduction is influenced by the particle-particle contact and, for the ZnO micro-varistor, also grain-boundary interface-physics.

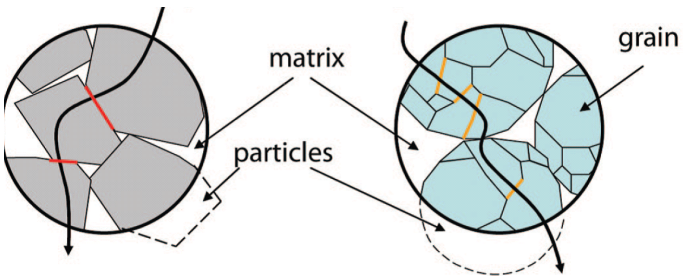

Figure 4.2: Sketches of two polymer volumes filled with SiC particles (left) and ZnO micro-varistor particles (right) [25]. Arrow: current path crossing micro-interfaces.

Three different nonlinear filled model material systems were studied:

- **Material A**: Silicone rubber filled with ZnO micro-varistor particles. The samples considered had thicknesses in the range 650-830 μm.
- **Material B**: ZnO varistor ceramics. The samples considered had thicknesses in the range 2.63-3.80 mm.

- **Material C**: Silicone rubber filled with SiC and carbon black. The samples considered had thicknesses in the range 295-435 μm.

These material systems were chosen since they were known to have a significant nonlinear behaviour. A more detailed description of the materials and their preparation is not provided, as the focus is on the characterization concept rather than on the properties of the specific materials.

4.2 Materials with macro-interfaces

This category comprises material systems where the nonlinearity is caused by macro-interfaces, like ion-blocking interfaces or charge injecting contacts. Within this category one system was studied:

- **Material D**: Sandwich system consisting of three material layers in series; polypropylene, Nafion (a proton conducting polymer), polypropylene. The systems considered had total thicknesses in the range 276-292 μm, of which each polypropylene film constituted about 9 μm.

This material system was studied with hope to achieve a nonlinear effect due to the ion-blocking interfaces between the insulating polypropylene and the proton conducting Nafion.

When studying systems that are assembled of a series of materials there are some relations that can be of use. It is well known that the total impedance Z_{tot} of a system with n components in series is given by

$$Z_{tot} = \sum_n Z_n \tag{4.1}$$

where Z_n is the impedance of the nth component. In the case of large contact (or interface) impedance, one also has to include the corresponding impedance in the sum in equation (4.1). Furthermore, the impedance is the inverse of the admittance G, which can sometimes be expressed in terms of the real permittivity and the real conductivity,

$$G = \frac{A}{L}(\sigma^{'} + i\omega\epsilon_0\epsilon^{'}). \tag{4.2}$$

However, note that the conductivity or permittivity of an assebled system can in general not be determined from knowing the properties of its components. Particularly at low frequencies or DC the electric behaviour is a system behaviour. There can be synergetic effects, where the system shows properties that can not be described as a sum of its components. For instance, the perfect insulator without intrinsic carriers (see section 2.2.5) which exhibits space charge limited currents with finite conductance, although the bulk conductivity of the material alone is $\sigma = 0$.

5

Experimental results

This chapter contains experimental results from the different IS measurements. To study the consistency, some IS results are compared to results from IV-setup 1 and IV-setup 2. The material systems are presented one after another in separate sections, starting with Material A. Note that the experiments were carried out with the aim to investigate the potential of the nonlinear IS methods, and not to thoroughly characterize the considered material systems.

5.1 Material A

This material has a relatively high conductivity (in the context of insulation systems) and shows good reproducibility. Small-amplitude IS measures the complex dielectric constant ϵ^* (or equivalently the complex conductivity σ^*). Figure 5.1 shows the frequency behaviour of the real permittivity and the real conductivity for Material A. Results of the dielectric loss (ϵ'') and tangent delta ($\tan(\delta) = \epsilon''/\epsilon'$) can be found in Appendix B.

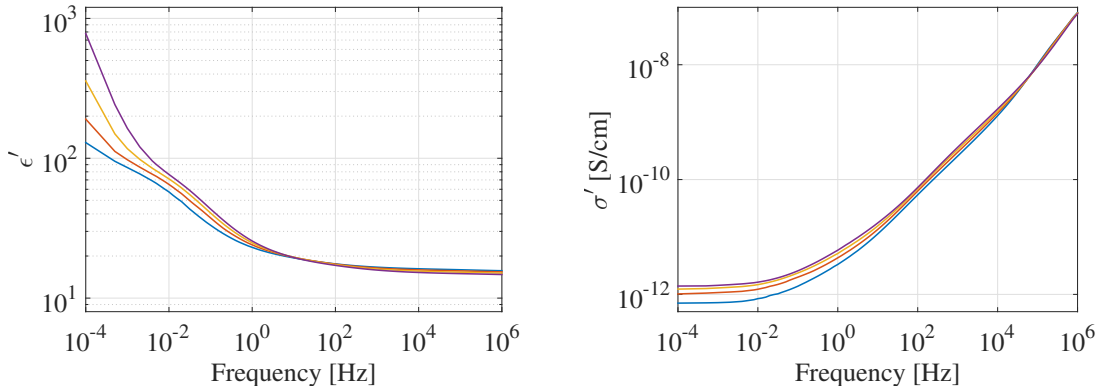

(a) **(b)**

Figure 5.1: The frequency behaviour of the real permittivity (ϵ') and the real electrical conductivity (σ') for Material A measured at a voltage of 1 V rms for temperatures T = 30 °C (blue), 40 °C (red), 50 °C (yellow), 60 °C (purple).

As can be seen in figure 5.1a, ϵ' has a plateau at high frequencies. Furthermore,

according to figure 5.1b, the conductivity $\sigma^{'}$ reaches a plateau for frequencies below f $\approx 10^{-2}$ Hz. From this "DC plateau" one obtains the value of the zero-frequency small-field conductivity, or the "DC-conductivity" value. To investigate the temperature dependence of the DC conductivity, the data was fitted to the Arrhenius law,

$$\sigma = \sigma_0 e^{-W/kT} \tag{5.1}$$

and the Vogel-Fulcher-Tammann (VFT) law,

$$\sigma = \sigma_0 e^{-A/(kT-kT_0)} \tag{5.2}$$

where σ_0 is a constant, W the activation energy, k the Boltzmann constant, T the absolute temperature, T_0 the Vogel temperature [26] and A a material parameter that is related to the activation energy (for $T_0 = 0$ the VFT law is simply the Arrhenius law and $A = W$). Figure 5.2 shows the data fitted to the two laws and here it is obvious that a VFT law fits the data much better. The VFT law resulted in $A = 1.6$ meV and a Vogel temperature $T_0 = 285.4$ K, while the Arrhenius fit would yield an activation energy of W = 0.21 $\pm$ 0.11 eV. The good fit of the data to the VFT law may indicate that the material experience a glass transition. However, the Vogel temperature T_0 is a fitting parameter and does not necessarily have the same value as the glass transition temperature. It is difficult to draw any conclusions about the temperature dependence of the DC conductivity for this material without further investigations, but since this is not the main focus of this work it will not be discussed in more detail here.

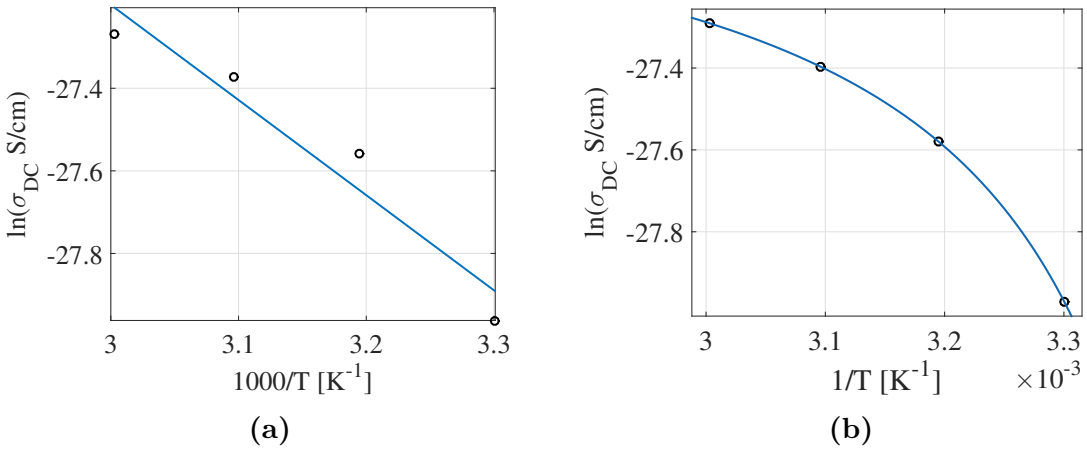

Figure 5.2: Temperature dependence of the DC conductivity fitted to (a) an Arrhenius law and (b) a Vogel-Fulcher-Tammann law.

Next, the consistency of the HV IS and current-voltage (I-V) measurements was studied. Because of the strong dependence of DC current measurements on the specific details of the experimental setup and its environment, two different equipments

(IV-setup 1 and IV-setup 2, see chapter 3 for details) were used in addition to the IS.

In figure 5.3 we show a typical final summarizing result for two different temperature values. The values obtained from setup 1 are indicated by the star symbols. The time dependent current results from setup 1 are shown in figure 5.4 (or Appendix B for separate graphs including more details). The I-V characteristics from IV-setup 2 is shown by the grey curve. The black curve is reconstructed from the differential conductivity. During some of the current measurements with IV-setup 1 at 60 °C the current increased unexpectedly with time (see figure B.3). Therefore both minimum values (red stars) and the last measured values (green stars) are plotted. The reason of this increase is unclear, it might have to do with thermal effects.

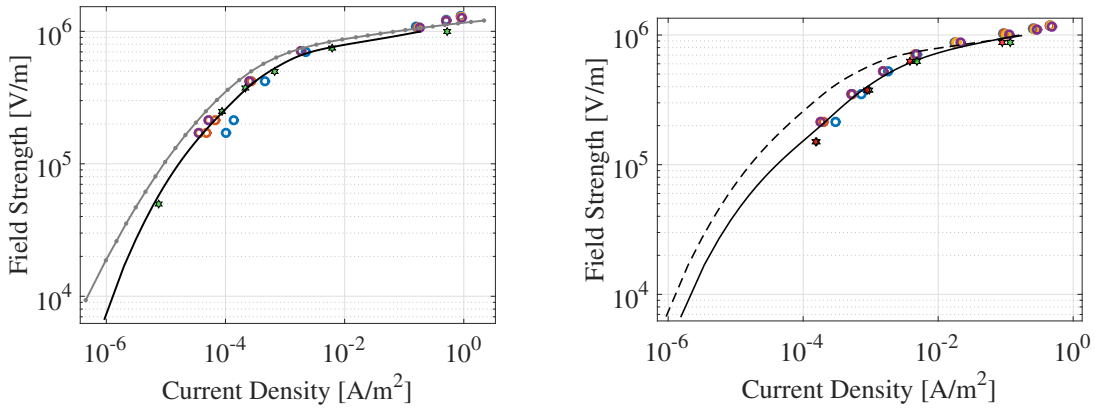

Figure 5.3: Overview of the material characteristics for Material A determined with the different methods at (a) 30 °C and (b) 60 °C. Circles: IS (blue: 1 Hz, red: 100 mHz, yellow: 10 mHz, purple: 1 mHz); stars: IV-setup 1; grey curve: IV-setup 2; black curve: reconstruction from AC-DC superposition. The red stars in (b) are explained in the text and the dashed curve corresponds to the black curve at 30 °C in (a).

In total, three different samples were tested with IV-setup 2 for this material and the results were reproducible. Higher harmonics measurements with the IS setup and measurements with IV-setup 1 were however only performed on one sample each.

Overall, the results in figure 5.3 from the different measuring techniques are in close agreement with each other. As one expects, there is a temperature dependence with positive dj/dT at low fields (i.e. in the insulating region where thermal activation may dominate) while it seems to become negative at high fields (in the conductive region where material expansion and separation of filler particles may play a role).

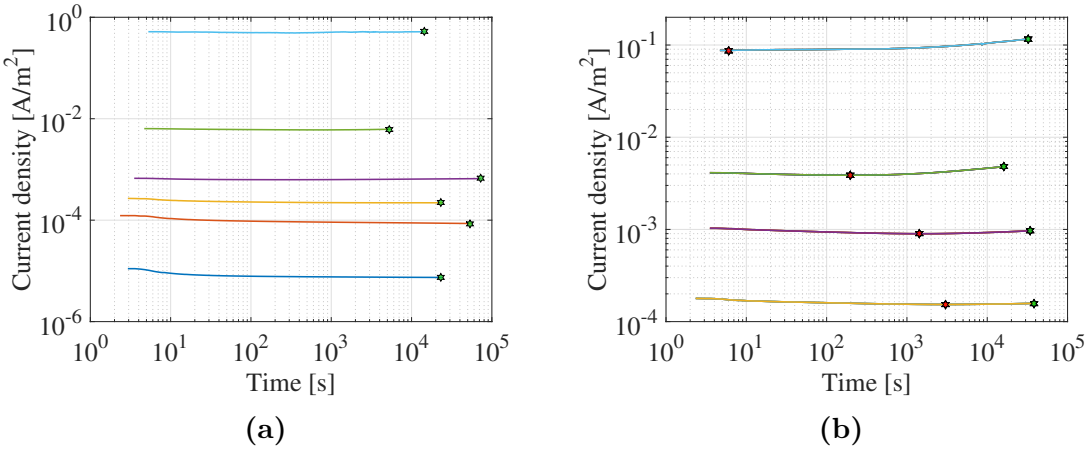

Figure 5.4: Polarization current measurements over time with IV-setup 1 at (a) 30 °C for fields 0.05, 0.25, 0.375, 0.50, 0.75, 1 kV/mm and (b) 60 °C for fields 0.15, 0.375, 0.625, 0.875 kV/mm.

The differential conductivity $\sigma_D = dj/dE$ (used to reconstruct the black curves in figure 5.3a and 5.3b) was determined from the low-frequency linear response and can be seen as a function of the field stength in figure 5.5 for 30 °C and 60 °C. The circles in figure 5.3a show measured values for two different AC fields at f = 10 mHz, where the plateau was already reached (see figure 5.1b). The circles corresponding to the superimposed AC-DC measurement and one additional point measured with the small signal IS at 1.7 V/mm (without superimposed DC field) were interpolated using a smoothing spline function (black curve in figure 5.5).

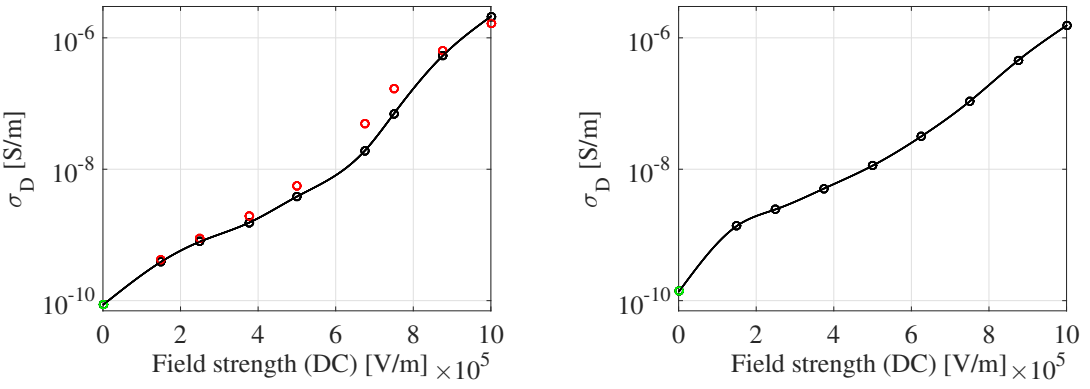

Figure 5.5: Differential conductivity as a function of the DC field strength for Material A at (a) 30 °C and (b) 60 °C. Circles: IS measurements with small-signal AC voltage superimposed to a DC voltage (AC voltage: $1.7 \cdot 10^{-3}$ kV/mm (green), 0.021 kV/mm (black), 0.21 kV/mm (red)). Solid line: spline fit.

The total current from the HV IS measurements of the higher harmonics was calculated from the sum of the first, third and fifth harmonic for different voltage amplitudes (in accordance with equation 3.2 for highest harmonic $N = 5$). Figure

5.6 shows, for four different field values on the characteristics, the first few superharmonic amplitudes normalized to the value of the fundamental frequency. Since the frequencies were normalized individually, the harmonic corrensponding to $k = 1$ equals one for all frequencies and therefore only one bar is shown for k = 1 in the figure. The harmonic contributions will be presented in the same way for the other material systems as well. All these superharmonic amplitudes correspond to the in-phase current response and hence (in the DC limit) the conduction current. The absolute current amplitudes for the fundamental frequency can be found in table B.1 in Appendix B. As can be seen in figure 5.6 the higher harmonics constitute a significant part of the total current.

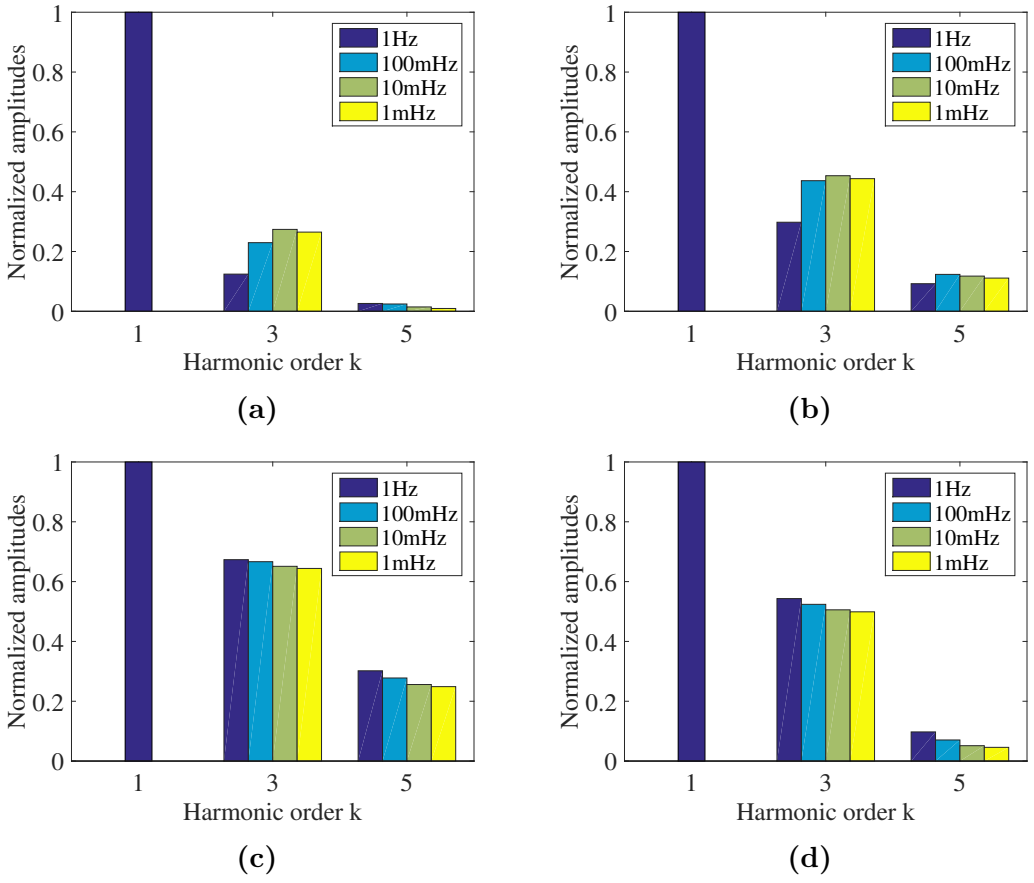

Figure 5.6: Material A: conduction currents ($I_k^{'}$) of each harmonic (normalized with respect to the first harmonic) for four different field values; (a) 0.4 kV/mm (b) 0.7 kV/mm (c) 1.1 kV/mm and (d) 1.2 kV/mm. Absolute values of the amplitudes corresponding to the fundamental frequencies can be found in section B.1 in appendix B.

From figure 5.3a it is clear that for smaller (angular) frequencies ω the HV IS circles shift to smaller currents. As can be seen, the current densities show a stronger frequency dependence for lower field amplitudes while above $E_0 \approx 10^6$ V/m they are more or less frequency independent. Furthermore, the resulting current is not changing significantly between 1 mHz and 10 mHz anywhere in the field region considered, indicating that the DC plateau is reached.

In summary, we may say that the different methods are in close agreement with each other and the nonlinear IS reproduce well the current field characteristics of the field grading material.

5.2 Material B

The analogous results as presented for Material A are now shown for Material B. The small signal response (U = 1 V rms) of the real permittivity (ϵ') and the real electrical conductivity (σ') are given in figure 5.7 for temperatures T = 30 °C - 200 °C. As one expects, the conductivity value of the DC plateau and the frequency value until which the plateau extends increase with temperature. Again, results of the dielectric loss (ϵ'') and tangent delta ($\tan(\delta) = \epsilon''/\epsilon'$) can be found in Appendix B (figure B.4).

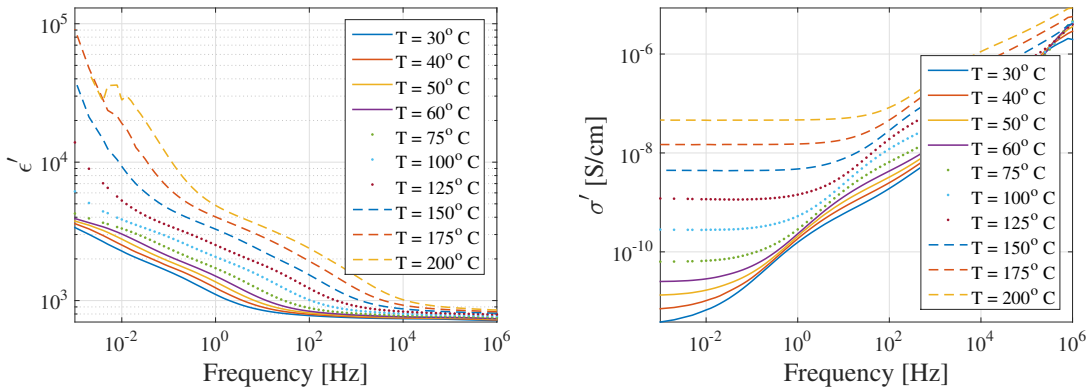

(a) **(b)**

Figure 5.7: The frequency behavior of the real permittivity (ϵ') and the real electrical conductivity (σ') for Material B measured at a voltage of 1 V rms for temperatures T = 30 °C - 200 °C.

In contrast to Material A, here an Arrhenius law seems to hold (see figure 5.8) with an activation energy of $W = 0.69\,\text{eV}$. This seems reasonable since Material A is based on a rubber, where glass transition like behaviour is often observed, while Material B is a ceramic. The conductivity values were taken at f = 1 mHz where the plateau was reached for all temperatures (see figure 5.7b).

The current-field characteristics calculated from nonlinear HV IS measurements including higher harmonics at 30 °C and frequencies f = 1 mHz, 10 mHz, 100 mHz and 1 Hz and AC-DC superimposed IS, together with measurements from the two IV setups is shown in figure 5.9a. This figure is analogous to figure 5.3a for Material A. Again, the experiments were performed at the temperature 30 °C for the IV-setup 1 and the IS measurements, and at room temperature for IV-setup 2. The current measurements as a function of time from IV-setup 1 can be found in figure 5.10a (for more details see Appendix B, figure B.5).

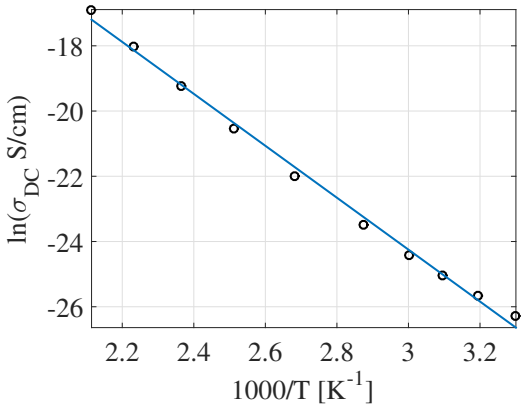

Figure 5.8: Arrhenius fit for Material B with activation energy 0.69 eV.

Material B shows a much stronger frequency dependence than Material A. The IS measurements at the lowest frequency, 1 mHz, are in impressively close agreement with the results from AC-DC superimposed IS and the results from IV-setup 1. The higher current from setup 2 is probably due to the limited time step between the measurements.

Equivalent results of current-field characteristics at 100 °C are shown in figure 5.9b. Again, measurements with IV-setup 1 can be found in figure 5.10b (or more detailed in Appendix B, figure B.6). Also at this temperature the IS measurements of higher harmonics at the lowest frequency are in close agreement with both the results from superimposed AC-DC IS as well as the results from IV-setup 1.

As well as for Material A, three different samples were tested with IV-setup 2 and the results were reproducible. Measurements of higher harmonics with the IS setup and measurements with IV-setup 1 were only performed on one sample each.

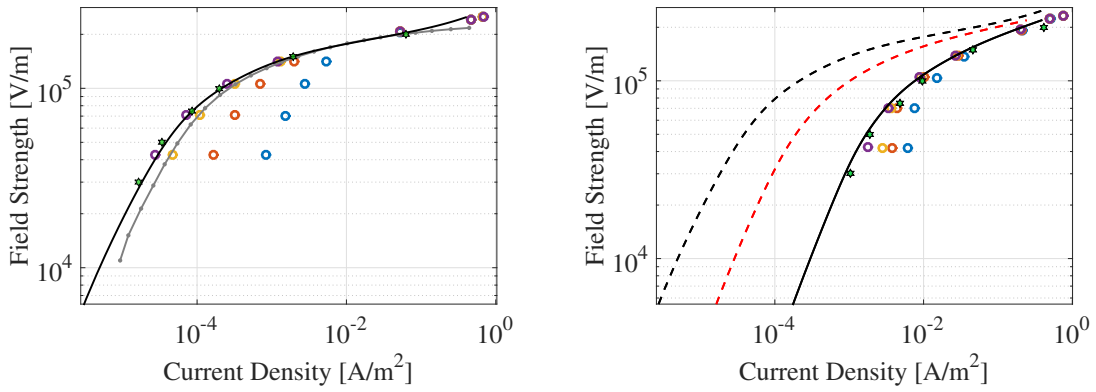

Figure 5.9: Comparison of the current-field characteristics for Material B at (a) 30 °C and (b) 100 °C. Circles: IS (blue: 1 Hz, red: 100 mHz, yellow: 10 mHz, purple: 1 mHz); stars: IV-setup 1; grey curve: IV-setup 2; black curve: reconstruction from AC-DC superposition. Dashed lines in (b) reconstructed from σ_D at 30 °C (black) and 60 °C (red).

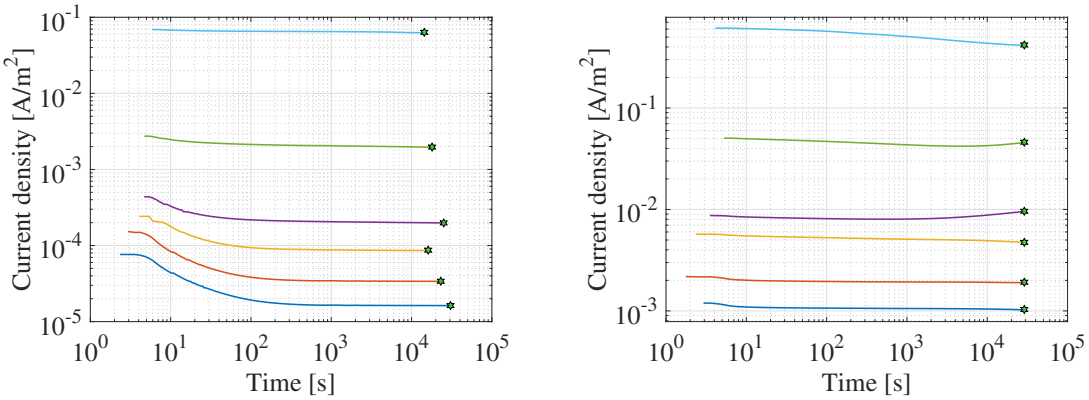

Figure 5.10: Current measurements over time with IV-setup 1 at (a) 30 °C and (b) 100 °C for fields 0.03, 0.05, 0.075, 0.1, 0.15, 0.2 kV/mm.

The differential conductivity as a function of the DC field strength at 30 °C and 100 °C is shown in figure 5.11 (results for 60 °C can be found in figure B.7 in Appendix). These results were obtained from AC-DC superimposed IS and used to reconstruct the I-V characteristics shown in figure 5.9, in the same way as for Material A.

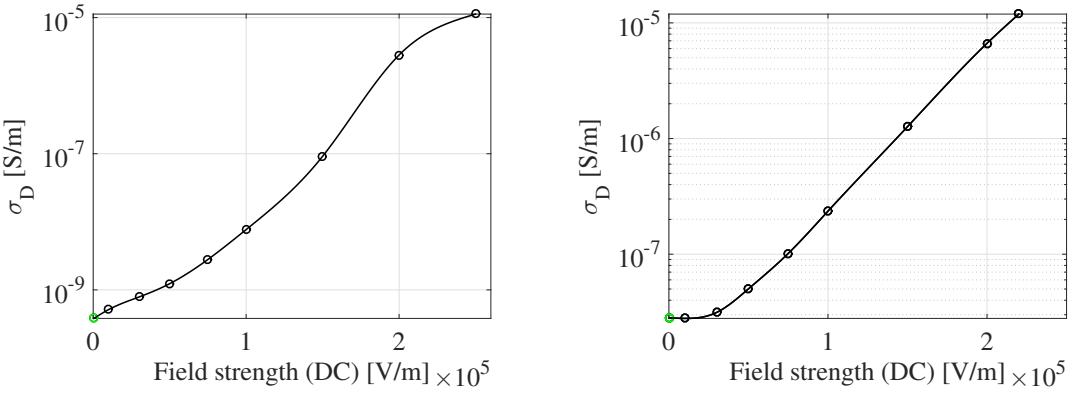

Figure 5.11: Differential conductivity as a function of the DC field strength for Material B at (a) 30 °C and (b) 100 °C. Circles: IS measurements with small-signal AC voltage superimposed to a DC voltage (AC voltage: 0.38 $\cdot 10^{-3}$ kV/mm (green), 3.8 $\cdot 10^{-3}$ kV/mm (black)).

Figure 5.12 shows the normalized current contributions I_k' of the superharmonics for four different field values. As well as for Material A, the current contributions from the third and fifth harmonics are significant. The absolute current amplitudes for the fundamental frequency can be found in table B.2 in Appendix B.

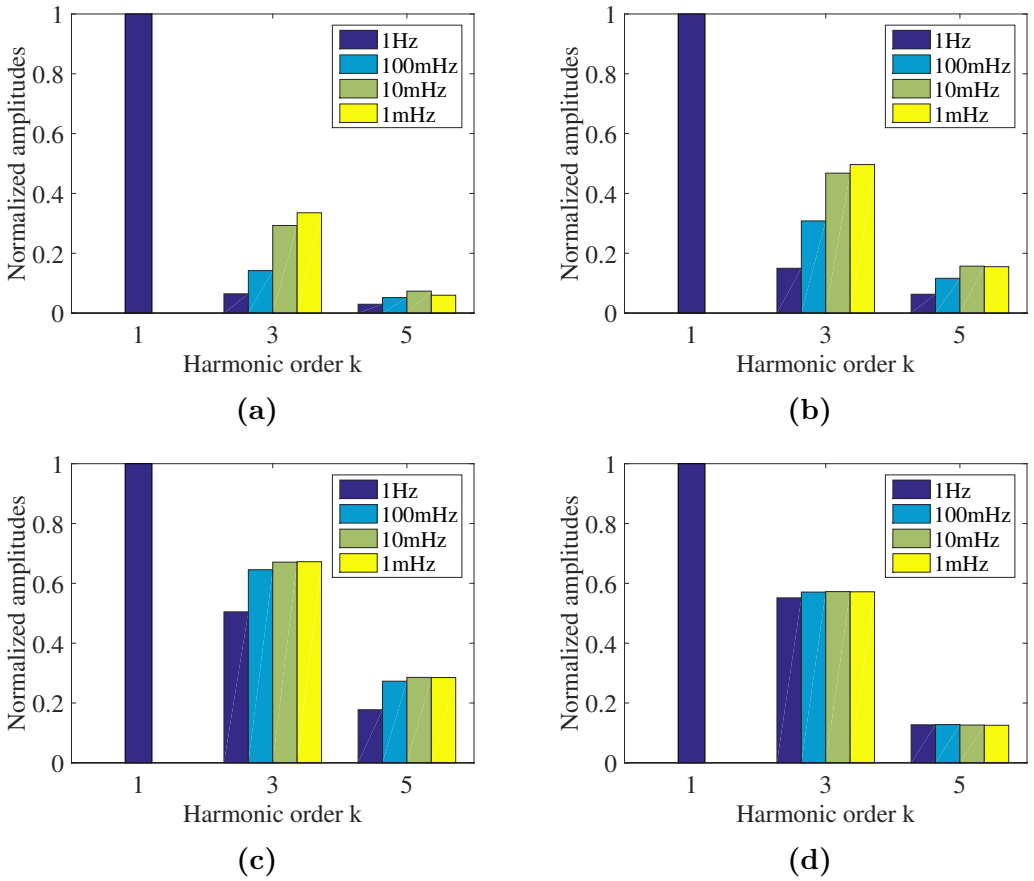

Figure 5.12: Material B: conduction currents ($I_k^{'}$) of each harmonic (normalized with respect to the first harmonic) for four different field values; (a) 0.11 kV/mm (b) 0.14 kV/mm (c) 0.21 kV/mm and (d) 0.24 kV/mm. Absolute values of the amplitudes corresponding to the fundamental frequencies can be found in section B.2 in appendix B.

5.3 Material C

This material turned out to be inappropriate for a characterization with the present methods, at least for reasonable experiment times and frequencies. However, from this one can learn about the applicability of the electrical characterization methods, which is not always possible e.g. if the insulation material behaviour is not robust. Figure 5.13 shows the frequency behaviour of the real permittivity ($\epsilon^{'}$) and the real electrical conductivity ($\sigma^{'}$) (for $\epsilon^{''}$ and $\tan(\delta)$ see Appendix B). The permittivity is slightly decreasing with increasing temperature, which is in general not obvious for a field grading material. The physical origin to this negative temperature dependence is not clear, but similar behaviour has been observed before in polymers [27, 28]. One possible explanation could be thermal expansion of the material. However, the coefficient of thermal expansion for silicone rubber is 2.5-3·10^{-4} K^{-1} [29], which is not high enough to cause a change of the sample thickness that would explain this difference. Nevertheless, an expansion of the silicone rubber could result in the material being "squeezed". This could lead to changes in the material structure

on a microscopic level, such as separation/reorientation of SiC and carbon black particles, which governs the permittivity. Note also that the expansion mechanics is not so simple since the sample is kept between two electrodes.

Another noticeable difference between this material system and the previously considered systems is that the conductivity is considerably lower. The conductivity of Material C is around 2-4 orders of magnitude lower than of Material A and of Material B. Furthermore, this system behaves qualitatively like an insulator and exhibits, particularly at low temperatures (< 60-70 °C), a long equilibration time.

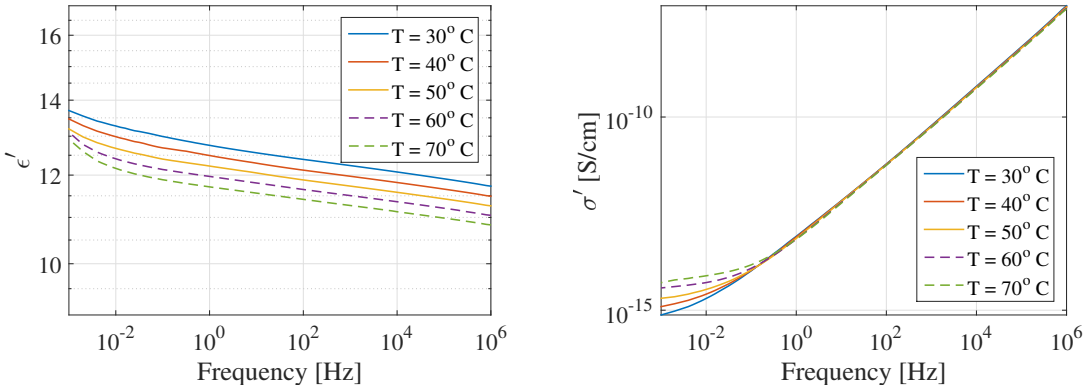

Figure 5.13: The frequency behavior of the real permittivity (ϵ') and the real electrical conductivity (σ') for Material C measured at a voltage of 1 V rms for temperatures T = 30 °C - 70 °C.

The 30 °C current-field dependence from the various measurements is shown in figure 5.14. The polarization current measurements, as well as the differential conductivity, can be found in the Appendix B. It is clear from figure 5.14 that consistency between the measurements cannot be expected because a reasonable DC steady state was not reached yet. Particularly the time duration of setup 2 is inappropriate and leads to much too high current prediction for a DC measurement.

For this material, five different samples were tested with IV-setup 2 and the deviation between the results was significant (in figure 5.14 only one of these curves is shown). This could be caused by variations between the samples or by the lack of robustness of this material. Measurements of higher harmonics with the IS setup were performed for two different samples with similar results. With IV-setup 1 two samples were measured with large deviations of the results. However, the deviations were not systematic and it is difficult to say whether the reason is sample variations or the generally non-robust nature of the material.

The conductivity values for the differential conductivity from the AC/DC superposition were taken at f = 1 mHz, the lowest frequency measured; the DC plateau was not reached. The reconstructed I-V (solid black curve in figure 5.14) also differs strongly from the other results. The actual differential conductivity is in fact smaller than the one used to reconstruct the current-voltage characteristics, which leads to this instability to predict steady state values.

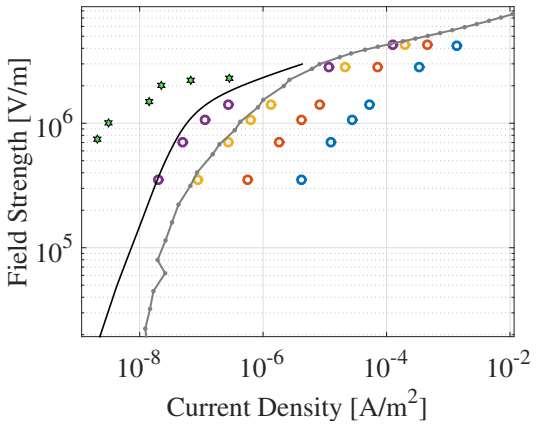

Figure 5.14: Overview of the current-voltage characteristics for Material C at 30 °C. Circles: IS (blue: 1 Hz, red: 100 mHz, yellow: 10 mHz, purple: 1 mHz); stars: IV-setup 1; grey curve: IV-setup 2; black curve: reconstruction from AC-DC superposition.

In figure 5.15 the normalized current contributions for the first, third and fifth harmonics are shown for two different field strengths. Even for this material system the higher harmonics play an important role, especially at small frequencies. The amount of the current contained in the higher harmonics depends strongly on frequency.

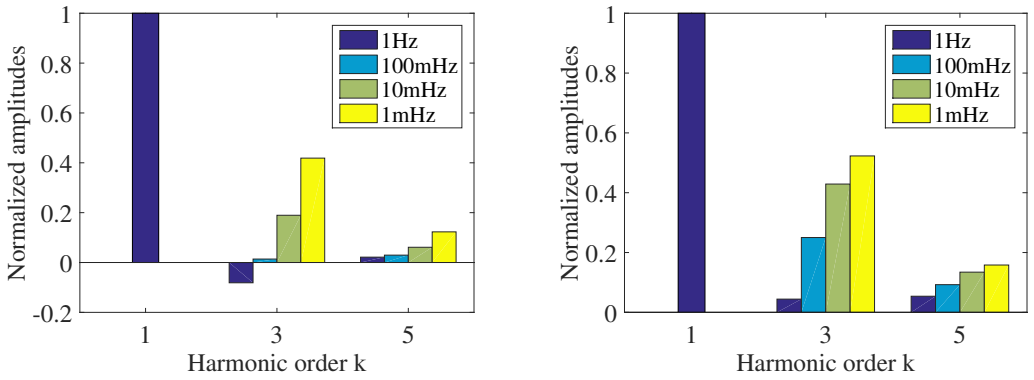

Figure 5.15: Material C: conduction currents (I_k') of each harmonic (normalized with respect to the first harmonic) for two different field values; (a) 1.4 kV/mm and (b) 2.8 kV/mm. Absolute values of the amplitudes corresponding to the fundamental frequencies can be found in section B.3 in appendix B.

One may conclude that a characterization of this material requires much longer measurement times/lower frequencies which is inconvenient for the purpose of this study.

5.4 Material D

This material system consists of a Nafion sample "sandwiched" between two thin polypropylene films and was investigated with the hope to observe nonlinearities due to the interfaces between the Nafion and the polypropylene films. However, the system turned out to be inappropriate for this study. The measurement results are not reproducible and the data can not be trusted. For completeness the results are presented in a similar manner as for the previously considered systems.

Figure 5.16 shows the frequency behavior of the real permittivity (ϵ') and the real electrical conductivity (σ') of the complete material system and its components; a Nafion sample and two layers of polypropylene films. Results of ϵ'' and $\tan(\delta)$ can again be found in Appendix B. As can be seen, a DC plateau was never reached for the considered frequencies.

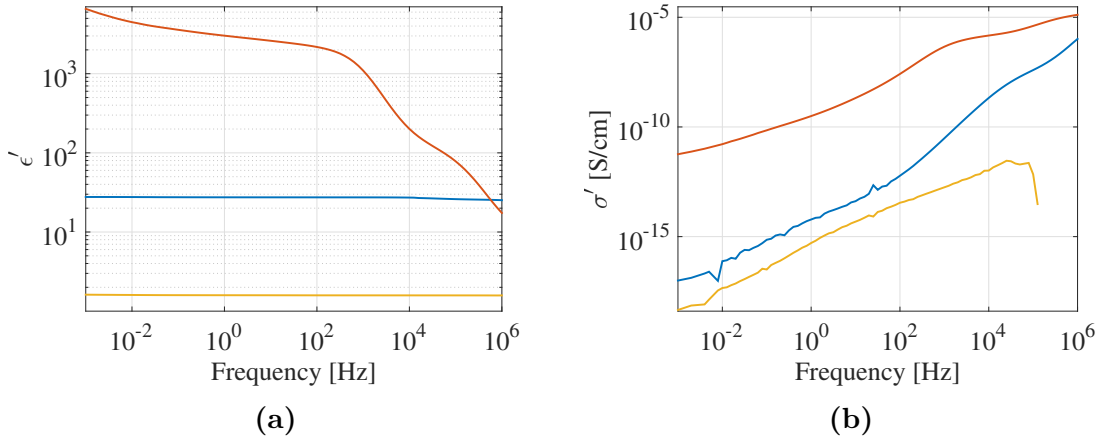

Figure 5.16: The frequency behavior of the real permittivity (ϵ') and the real electrical conductivity (σ') for the complete material system (blue), a Nafion sample (red) and two layers of polypropylene films (yellow), measured at a voltage of 1 V rms at 30 °C.

The current-field dependence from IS measurements of higher harmonics is shown in figure 5.17a together with results from two measurements with IV-setup 1. The IS measurements were performed twice for the same material system at frequencies 10 mHz and 1 Hz, and the results are clearly not reproducible. Material systems consisting of other samples were also measured but non of the results are consistent with each other. Results from the polarization current measurements can be found in figure 5.17b. These measurements were performed on two different samples, and non of them are the same sample as was used for the HV IS in figure 5.17a. Since a reasonable DC steady state was never reached for the measurements with setup 1, consistency with the IS measurement cannot be expected.

For this material system three different "sandwiches" were measured with the IS setup, without consistency between any of the results. The results shown in figure 5.17a are from two different measurements on the same system of samples.

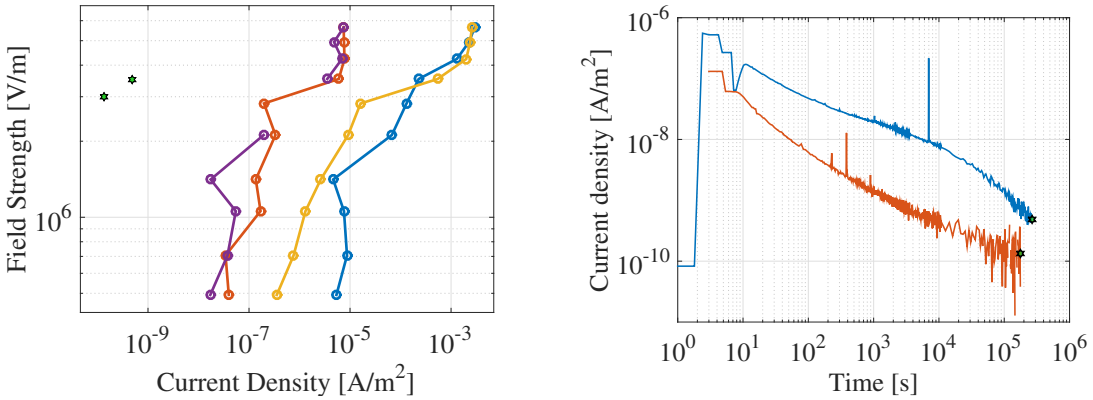

(a) **(b)**

Figure 5.17: Material D: (a) Current-voltage characteristics at 30 °C. Circles: IS (blue: 1 Hz, red: 10 mHz, yellow: 1 Hz, purple: 10 mHz); stars: IV-setup 1. (b) Current measurements over time with IV-setup 1 at 30 °C for fields 3 kV/mm and 3.5 kV/mm.

The behaviour of the superharmonic amplitudes varies a lot between the different field strengths. In figure 5.18 the normalized current contributions for the odd harmonics up to the ninth superharmonic are shown for two different field strengths as an example. The absolute values of the current density amplitudes corresponding to the fundamental frequencies can be found in section B.4 in appendix B.

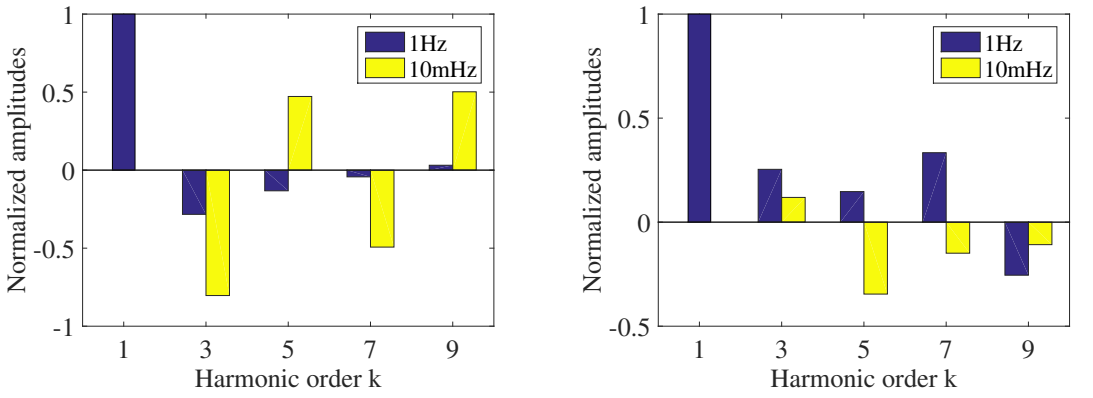

(a) **(b)**

Figure 5.18: Material D: conduction currents (I_k') of each harmonic (normalized with respect to the first harmonic) for two different field values; (a) 0.49 kV/mm and (b) 2.1 kV/mm.

Despite that the superharmonics appear to vary randomly, the time dependent current behaviour (reconstructed from the measured superharmonics) seems rather systematic. In figure 5.19 the time dependent behaviour is shown for the total current density and the in-phase current density for the six highest fields applied at the frequency 10 mHz. The corresponding time dependent applied field can be seen in

figure B.12 in Appendix B. The location of the peak of the periodic current is shifting with the field strength. This behaviour has not been observed for any of the other material systems.

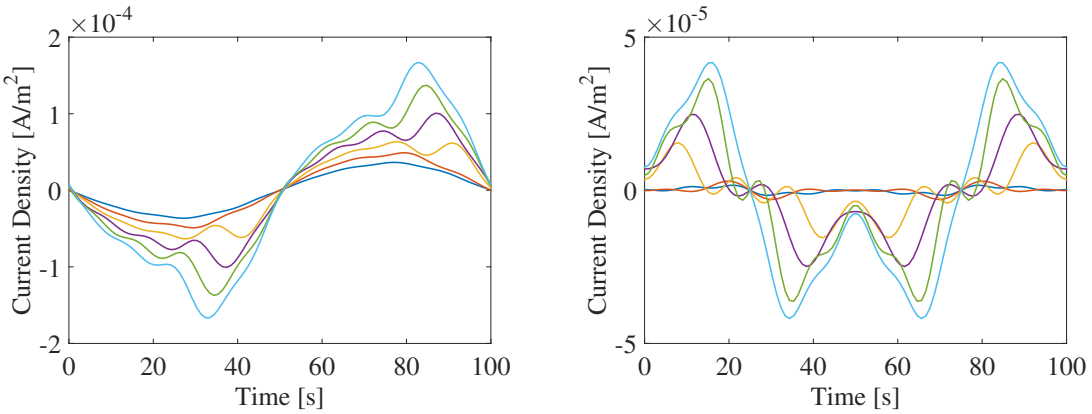

Figure 5.19: Time dependent current density reconstructed from measurements of higher harmonics at 10 mHz for Material D. (a) The total current density. (b) Current density calculated as a sum of the in-phase contributions j_k'.

To summerize, this material system is also not appropriate for the purpose of this work. One possible explanation for the inconsistency in the results is variations in humidity, which leads to differences in the amount of water contained in the Nafion.

6

Discussion and conclusions

This thesis aims to elaborate the potential of nonlinear IS for characterizing DC insulation materials. The steady state current-field relation was determined with different measurement methods for a few material systems. Overall, nonlinear IS techniques seem to be very useful for characterization of robust field grading materials.

If measurements of higher harmonics are performed at different fundamental frequencies and the results converge in the low frequency limit, this characterization method can most likely be used to determine the steady state current-field characteristics. Analogously, results from small amplitude AC spectroscopy at large superimposed DC seem to be trustworthy if the differential conductivity reaches the DC plateau in the considered frequency region.

The results for Material A and Material B show that the two nonlinear IS methods, higher harmonics measurement with high field impedance spectroscopy and differential conductivity measurement with small amplitude AC spectroscopy at large superimposed DC, work in principle with the given equipment (provided by Novocontrol Technologies). The results are reproducible and in good agreement with each other, and with IV-setup 1 (see figures 5.3 and 5.9). These two materials are robust and show nonlinear behaviour due to micro-interfaces.

For non-robust material systems, electrical characterization in general, and application of nonlinear IS in particular, is limited or even meaningless. Non-robust behaviour can for example occur for strongly sensitive materials and for systems that require very long times for relaxation to a steady state (i.e. strongly insulating systems). Sometimes insulation materials show electric behaviour that seems not to converge to a steady state at all within a reasonable measurement time. This was the case for Material C, which could not be uniquely characterized on the given time and/or frequency scales (see figure 5.14). A reason for the lack of robustness can be imperfect percolation of the filler particles. The lack of robustness is reflected in the missing convergence of the results in the limit $\omega \to 0$.

The attempt to observe nonlinearities due to the macroscopic interfaces in Material D was not successful. The results are not reproducible and the data can not be trusted (see figure 5.17a). One reason to that the system behaviour is not robust could be due to the properties of Nafion. It is known that this material is sensitive to variations in humidity and easily absorbs water [30, 31]. Its water content could not

be controlled during the measurements and this could have affected the electrical properties as well as the sample thickness (due to potential expansion related to the water uptake). Another reason of the instability in the results is likely that the highly insulating polypropylene films inhibit the possibility of reaching a steady state for the considered frequencies.

To further understand feasibility and limitations related to nonlinear IS it would be interesting to study a system where nonlinearity due to blocking macro-interfaces can be observed. Investigations of other kind of nonlinear material systems would also be useful, such as macro-interfaces where charge injection appear.

To summarize, we conclude that the two nonlinear IS techniques investigated are useful for electrical characterization of nonlinear materials under the condition that the studied systems are robust, and the frequency considered is so low that the insulation behaves quasi-static.

Bibliography

[1] F. Kreuger, *Industrial high voltage*. Delft: Delft University Press, 1995.

[2] T. Christen, 'Characterization and robustness of HVDC insulation.' *2013 IEEE International Conference on Solid Dielectrics (ICSD)*, Bologna, Italy, 2013.

[3] A. Jonscher, *Dielectric relaxation in solids.* London: Chelsea Dielectrics Press, 1983.

[4] J. Runt and J. Fitzgerald, *Dielectric spectroscopy of polymeric materials.* Washington, DC: American Chemical Society, 1997.

[5] F. Kremer and A. Schönhals, *Broadband dielectric spectroscopy.* Berlin: Springer, 2003.

[6] X. Qi, Z. Zheng and S. Boggs, 'Engineering with nonlinear dielectrics', *IEEE Electrical Insulation Magazine*, vol. 20, no. 6, pp. 27-34, 2004.

[7] J.Y. Zhou and S.A. Boggs, 'Measurement of nonlinear dielectric properties - effect of dielectric dispersion', in *Conference on Electrical Insulation and Dielectric Phenomena*, Kitchener, Ont., 2001, pp. 153 - 156.

[8] Y. Ishibashi, 'Nonlinear dielectric spectroscopy.' *Journal of the Korean Physical Society* vol. 32, pp. S407-S410, 1998.

[9] N. Taylor and H. Edin, 'Stator end-winding currents in frequency-domain dielectric response measurements', *IEEE Transactions on Dielectrics and Electrical Insulation*, vol. 17, no. 5, pp. 1489-1498, 2010.

[10] N. Taylor and H. Edin, 'Utilisation of voltage and frequency dependence of stress-grading materials in dielectric diagnostics', in *The 17th Annual Meeting of the IEEE Lasers and Electro-Optics Society*, 2004, pp. 178 - 181.

[11] A. Heuer, S. Murugavel and B. Roling, 'Nonlinear ionic conductivity of thin solid electrolyte samples: Comparison between theory and experiment', *Phys. Rev. B*, vol. 72, no. 17, 2005.

[12] C. Böttcher and P. Bordewijk, *Dielectrics in time-dependent fields*. Amsterdam: Elsevier Scientific Pub. Co., 1978.

[13] Novocontrol Technologies, *WinDETA 5.84 Owner's Manual*. Issue: 2, 2012.

[14] T. Christen, L. Donzel and F. Greuter, 'Nonlinear resistive electric field grading part 1: Theory and simulation', *IEEE Electrical Insulation Magazine*, vol. 26, no. 6, pp. 47-59, 2010.

[15] V. Tomer and C. Randall, 'High field dielectric properties of anisotropic polymer-ceramic composites', *J. Appl. Phys.*, vol. 104, no. 7, pp. 074106, 2008.

[16] T. Christen, 'HVDC insulation boundary conditions for modeling and simulation', *IEEE Transactions on Dielectrics and Electrical Insulation*, vol. 22, no. 1, pp. 35-44, 2015.

[17] N. F. Mott and R. W. Gurney, *Electronic processes in ionic crystals.* Oxford: Clarendon Press, 1940.

[18] M. A. Lampert, 'A simplified theory of two-carrier, space-charge-limited current flow in solids.' *RCA REVIEW*, no. 4, pp. 682-701, 1959.

[19] Novocontrol Technologies, 'Novocontrol Spectrometers for Dielectric Spectroscopy, Impedance Spectroscopy, and Electrochemical Impedance Spectroscopy', 2015. [Online]. Available: http://novocontrol.de. [Accessed: 03- Nov- 2015].

[20] Novocontrol Technologies, *Alpha-A High Resolution Dielectric, Conductivity, Impedance and Gain Phase Modular Measurement System User's Manual.* Issue: 7, 2012.

[21] Novocontrol Technologies, *High Voltage Test Interface HVB4000 for Alpha-A High Resolution Dilectric / Impedance Analyzer User's Manual.* Issue: 3, 2009.

[22] R. Kochetov, I.A. Tsekmes, P.H.F. Morshuis and J.J. Smit, 'Inaccuracies in the dielectric permittivity due to thickness variation', *IEEE Electrical Insulation Conference (EIC)*, Philadelphia, Pennsylvania, USA, 2014, pp. 55-58.

[23] Novocontrol Technologies, *WinTSC 1.47 Owner's Manual.* Issue: 5, 2011.

[24] L. Donzel, F. Greuter and T. Christen, 'Nonlinear resistive electric field grading Part 2: Materials and applications', *IEEE Electrical Insulation Magazine*, vol. 27, no. 2, pp. 18-29, 2011.

[25] T. Christen, L. Donzel, F. Greuter and M. Saltzer, 'Fundamentals of resistive field grading.' *ETG-Fachbericht-Feldsteuernde Isoliersysteme*, 2011.

[26] S.M. Musa, *Nanoscale Spectroscopy with Applications.* Boca Raton, Florida: CRC Press, 2013.

[27] R. Kochetov, I. Tsekmes and P. Morshuis, 'Electrical conductivity, dielectric response and space charge dynamics of an electroactive polymer with and without nanofiller reinforcement', *Smart Mater. Struct.*, vol. 24, no. 7, p. 075019, 2015.

[28] T. Christen, E. Logakis. 'The generic conduction model for solid polymer HVDC insulation material.' *Solid Dielectrics (ICSD), 2013 IEEE International Conference*, Bologna, Italy, 2013, pp. 1044 - 1047.

[29] Azom.com, 'Properties: Silicone Rubber', 2015. [Online]. Available: http://www.azom.com/properties.aspx?ArticleID=920. [Accessed: 25- Nov- 2015].

[30] G. Hwang, D. Parkinson, A. Kusoglu, A. MacDowell and A. Weber, 'Understanding Water Uptake and Transport in Nafion Using X-ray Microtomography', *ACS Macro Lett.*, vol. 2, no. 4, pp. 288-291, 2013.

[31] C. Yang, S. Srinivasan, J. Benziger, and A. B. Bocarsly. 'Water uptake and conductivity of composite membranes operating at reduced relative humidity.' *Electrochemistry Society 201*, 2001.

A

Appendix: Theory

This appendix contains calculations that complements the theory presented in chapter 2.

A.1 Example: Piecewise constant conductivity

In this section calculations of the current density amplitudes $j_1^{'}$ and $j_3^{'}$ are provided from the example with a piecewise constant conductivity presented in section 2.2.2.

$$\begin{aligned} j_1^{'} &= \tfrac{\omega}{\pi}\int_0^{2\pi/\omega} j(t)\cos(\omega t)\ dt = \tfrac{4\omega}{\pi}\int_0^{t_c}\sigma_0 E_0\cos^2(\omega t)\ dt = \\ &= \tfrac{4\omega}{\pi}\sigma_0 E_0\left[\tfrac{2t\omega+\sin(2\omega t)}{4\omega}\right]_0^{t_c} = \left\{\omega t_c = \arccos(\tfrac{E_c}{E_0})\right\} = \\ &= \tfrac{\sigma_0 E_0}{\pi}\left[2\arccos(\tfrac{E_c}{E_0}) + \sin(2\arccos(\tfrac{E_c}{E_0}))\right] \end{aligned} \tag{A.1}$$

$$\begin{aligned} j_3^{'} &= \tfrac{\omega}{\pi}\int_0^{2\pi/\omega} j(t)\cos(3\omega t)\ dt = \tfrac{2\omega}{\pi}\int_0^{\pi/\omega}\sigma_0 E_0\cos(\omega t)\cos(3\omega t)\ dt = \\ &= \tfrac{2\omega}{\pi}\sigma_0 E_0\left[\int_0^{t_c}\cos(\omega t)\cos(3\omega t)\ dt + \int_{\pi/\omega-t_c}^{\pi/\omega}\cos(\omega t)\cos(3\omega t)\ dt\right] = \\ &= \tfrac{\sigma_0 E_0}{4\pi}\left[4\sin(2\arccos(\tfrac{E_c}{E_0})) + 2\sin(4\arccos(\tfrac{E_c}{E_0}))\right] \end{aligned} \tag{A.2}$$

A.2 Example: Blocking electrodes

In this section Poisson's equation is solved for the example provided in section 2.2.4 with blocking electrodes. Thereafter it is shown that the average field is given by $\bar{E} = U/L$.

First we make an ansatz for the the electric potential field Φ in two different regions of the cross section area in figure 2.11a. Region I is located to the left of the charge sheet and region II to the right of the charge sheet, see equation A.3.

$$\begin{array}{lll} \text{Region I} & x \in [0, x_0[& \Phi_{\mathrm{I}}(x) = -\frac{q}{\epsilon}\left(-\frac{x^2}{2L} + C_1 x + D_1\right) \\ \text{Region II} & x \in]x_0, L] & \Phi_{\mathrm{II}}(x) = -\frac{q}{\epsilon}\left(-\frac{x^2}{2L} + C_2 x + D_2\right) \end{array} \tag{A.3}$$

From the continuity of the potential at x_0 ($\Phi|_{x_{0+}} = \Phi|_{x_{0-}}$), the discontinuity of the electric field at x_0 ($\Phi'|_{x_{0+}} - \Phi'|_{x_{0-}} = q/\epsilon$) and the boundary conditions $\Phi(0) = U$ and $\Phi(L) = 0$ one finds the following relations between the coefficients defined in equation A.3.

$$\begin{aligned} C_1 x_0 + D_1 &= C_2 x_0 + D_2 \\ C_1 - C_2 &= 1 \\ D_1 &= -\tfrac{\epsilon}{q} U \\ \tfrac{L}{2} - C_2 L - D_2 &= 0 \end{aligned} \tag{A.4}$$

From these four equations the four coefficients can be determined.

$$\begin{aligned} C_1 &= \tfrac{3}{2} - \tfrac{x_0}{L} + \tfrac{\epsilon U}{qL} \\ D_1 &= -\tfrac{\epsilon}{q} U \\ C_2 &= \tfrac{1}{2} - \tfrac{x_0}{L} + \tfrac{\epsilon U}{qL} \\ D_2 &= x_0 - \tfrac{\epsilon}{q} U \end{aligned} \tag{A.5}$$

Now the mean electric field can be calculated from the following equation.

$$\bar{E} = -\frac{1}{L}\left[\int_0^{x_0} \Phi_{\mathrm{I}}'(x) + \int_{x_0}^{L} \Phi_{\mathrm{II}}'(x)\right] \tag{A.6}$$

Inserting $\Phi_{\mathrm{I}}'(x)$ and $\Phi_{\mathrm{II}}'(x)$ into this equation gives the intuitive result $\bar{E} = U/L$.

B

Appendix: Experimental results

This appendix contains measurement results that complements the experimental results presented in chapter 5. The results are ordered by material system and presented one after another.

B.1 Material A

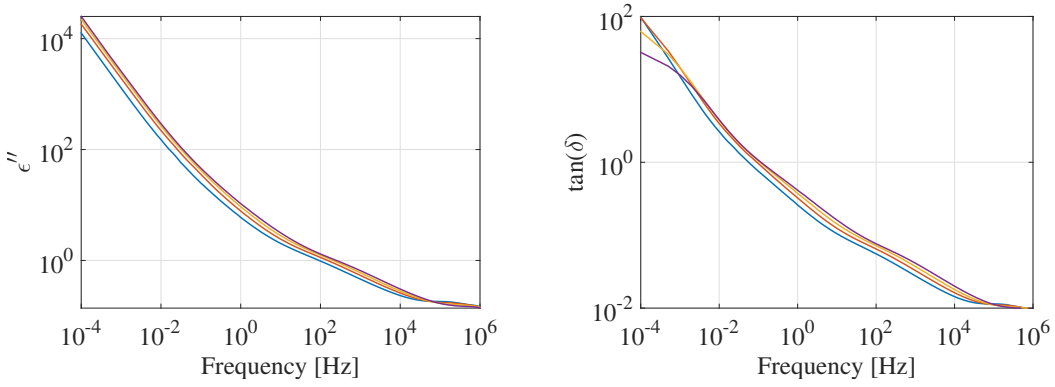

(a) **(b)**

Figure B.1: The frequency behavior of the dielectric loss (ϵ'') and tangent delta ($\tan(\delta) = \epsilon''/\epsilon'$) for Material A measured at a voltage of 1 V rms for temperatures T = 30 °C (blue), 40 °C (red), 50 °C (yellow), 60 °C (purple).

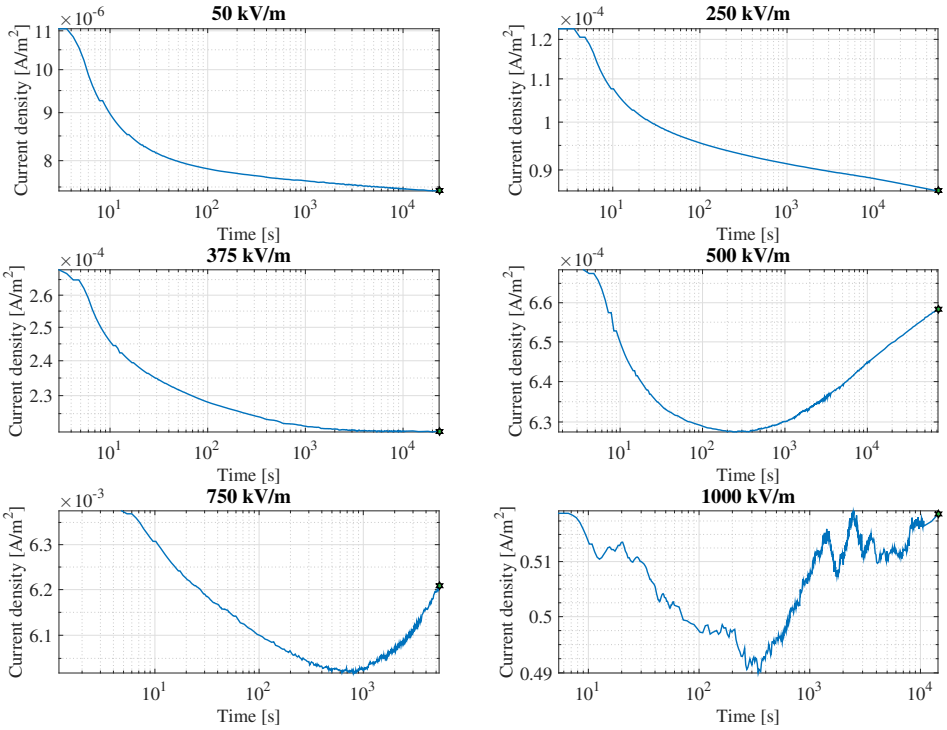

Figure B.2: Polarization currents of Material A measured with IV-setup 1 at 30 °C for different electric field values. The stars correspond to the stars in figure 5.3a. An increase of current density with time may be due to (local) Joule heating; however, the variations here are rather small.

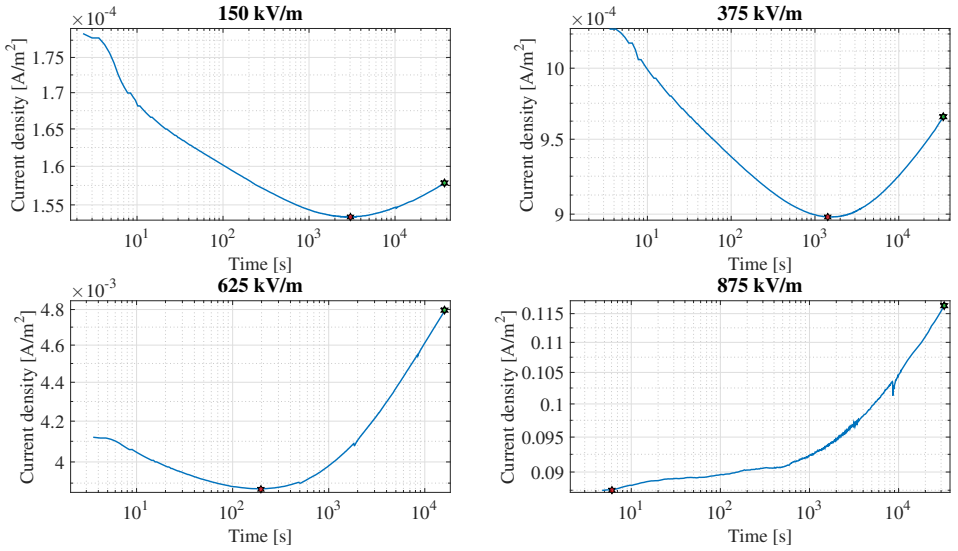

Figure B.3: Polarization currents of Material A measured with IV-setup 1 at 60 °C for different electric field values. The stars correspond to the stars in figure 5.3b.

Table B.1: Material A: Current density amplitudes of the fundamental frequency (j_1') in A/m^2 for different frequencies and field strengths.

Field Strength [V/m]	1 Hz	100 mHz	10 mHz	1 mHz
0.1697e06	9.5829e-05	4.3181e-05	3.2174e-05	3.0922e-05
0.2122e06	1.2601e-04	5.8985e-05	4.5762e-05	4.5056e-05
0.4226e06	4.0118e-04	2.1867e-04	1.9398e-04	1.9501e-04
0.7041e06	1.5816e-03	1.1767e-03	1.1587e-03	1.1850e-03
1.0777e06	7.9416e-02	8.6160e-02	9.2451e-02	9.5487e-02
1.2147e06	3.0489e-01	3.1463e-01	3.2334e-01	3.2625e-01
1.3020e06	6.1155e-01	6.3120e-01	6.5323e-01	6.5934e-01

B.2 Material B

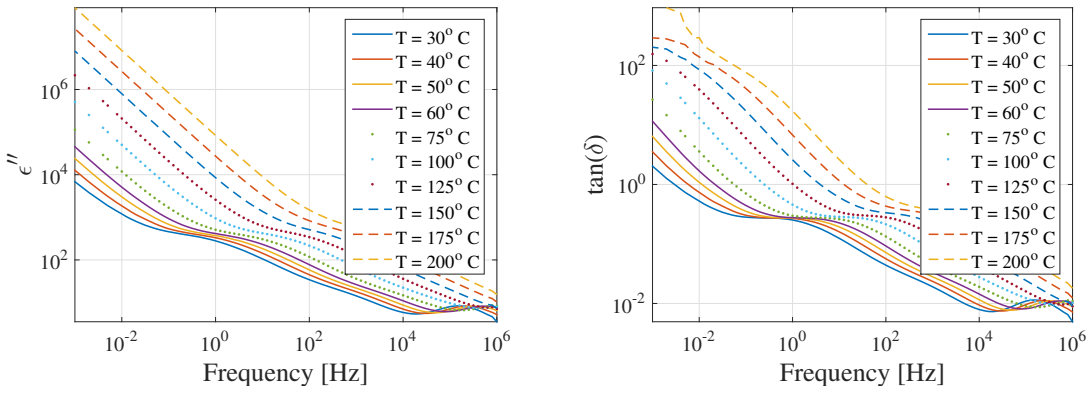

(a) **(b)**

Figure B.4: The frequency behavior of the dielectric loss (ϵ'') and tangent delta ($\tan(\delta) = \epsilon''/\epsilon'$) for Material B measured at a voltage of 1 V rms for temperatures T = 30 °C - 200 °C.

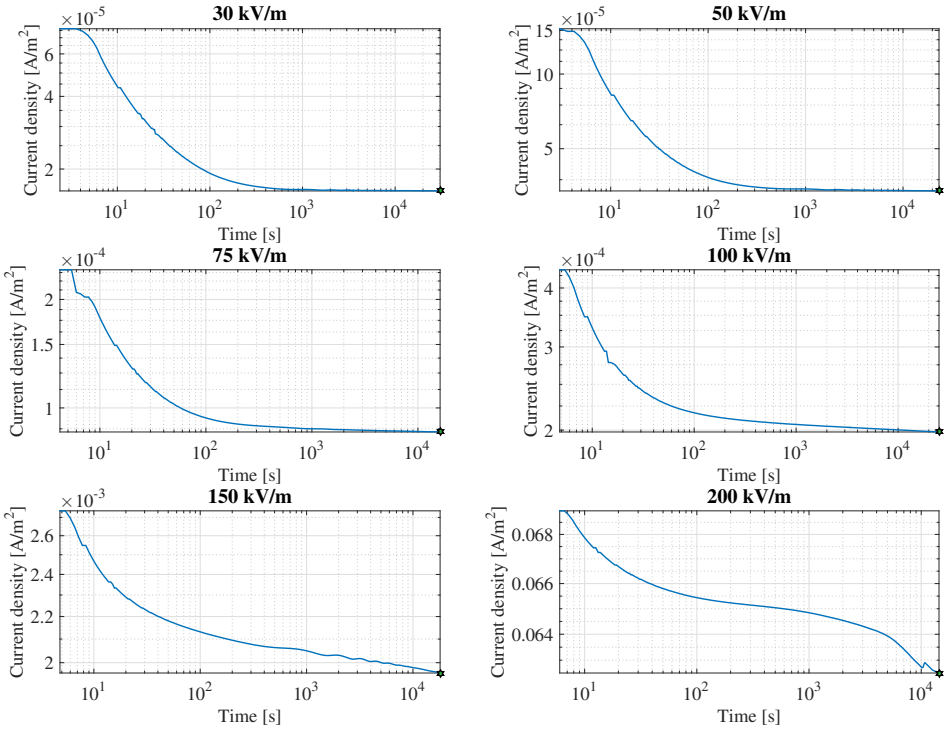

Figure B.5: Polarization currents of Material B measured with IV-setup 1 at 30 °C at different field values.

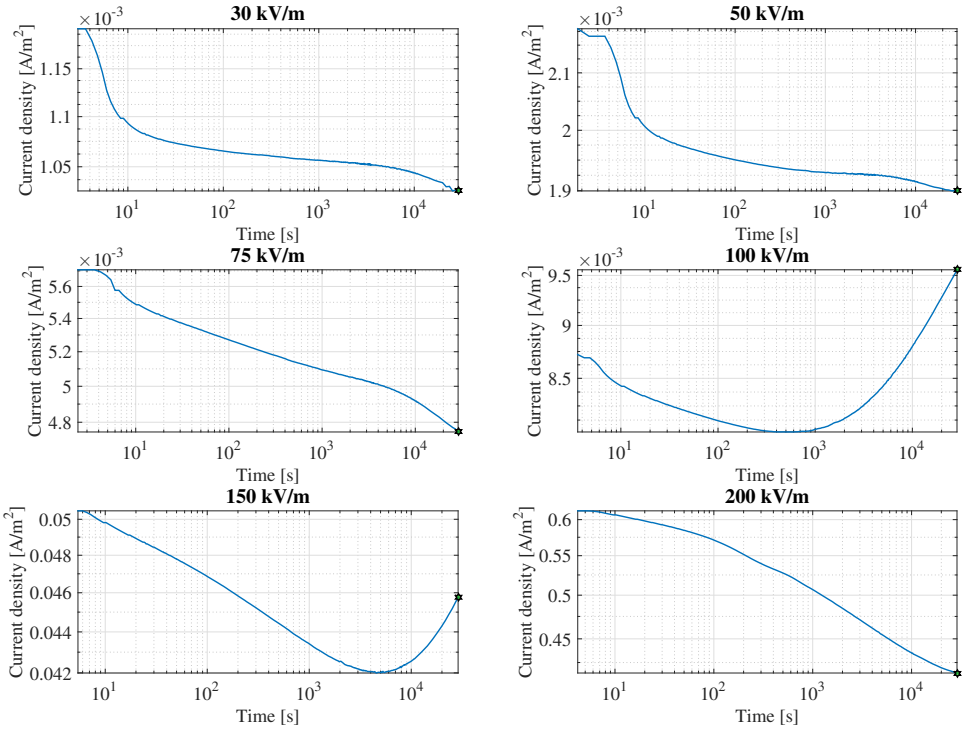

Figure B.6: Polarization current measurements from IV-setup 1 at 100 °C for Material B.

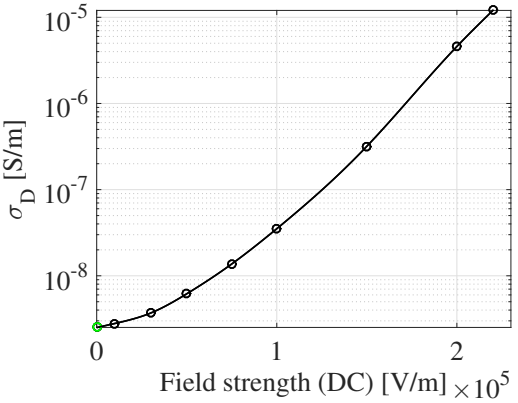

Figure B.7: Differential conductivity as a function of the DC field strength for Material B at 60 °C. Circles: IS measurements with small-signal AC voltage superimposed to a DC voltage (AC voltage: 0.38 V/mm (green), 3.8 V/mm (black)).

Table B.2: Material B: Current density amplitudes of the fundamental frequency (j_1') in A/m^2 for different frequencies and field strengths.

Field Strength [V/m]	1 Hz	100 mHz	10 mHz	1 mHz
0.4233e05	8.1909e-04	1.5769e-04	4.2288e-05	2.4764e-05
0.7053e05	1.4745e-03	2.9853e-04	9.0633e-05	5.9254e-05
1.0546e05	2.5429e-03	5.8961e-04	2.3619e-04	1.8277e-04
1.4038e05	4.4348e-03	1.3815e-03	8.1083e-04	7.2101e-04
2.0643e05	3.1240e-02	2.7376e-02	2.6747e-02	2.6714e-02
2.4195e05	2.8016e-01	2.7748e-01	2.7801e-01	2.7844e-01
2.5038e05	4.3468e-01	4.3470e-01	4.3589e-01	4.3682e-01

B.3 Material C

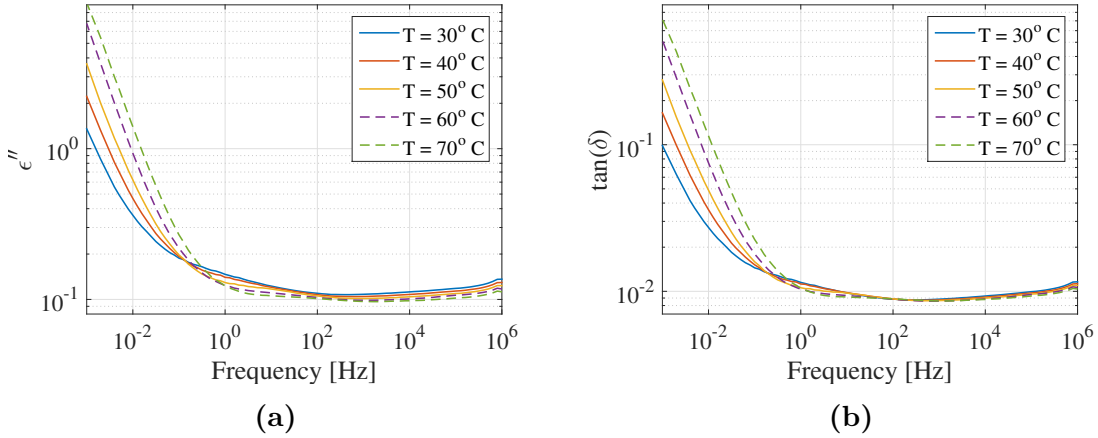

(a) **(b)**

Figure B.8: The frequency behavior of the dielectric loss (ϵ'') and tan(δ) for Material C measured at a voltage of 1 V rms for temperatures T = 30 °C - 70 °C.

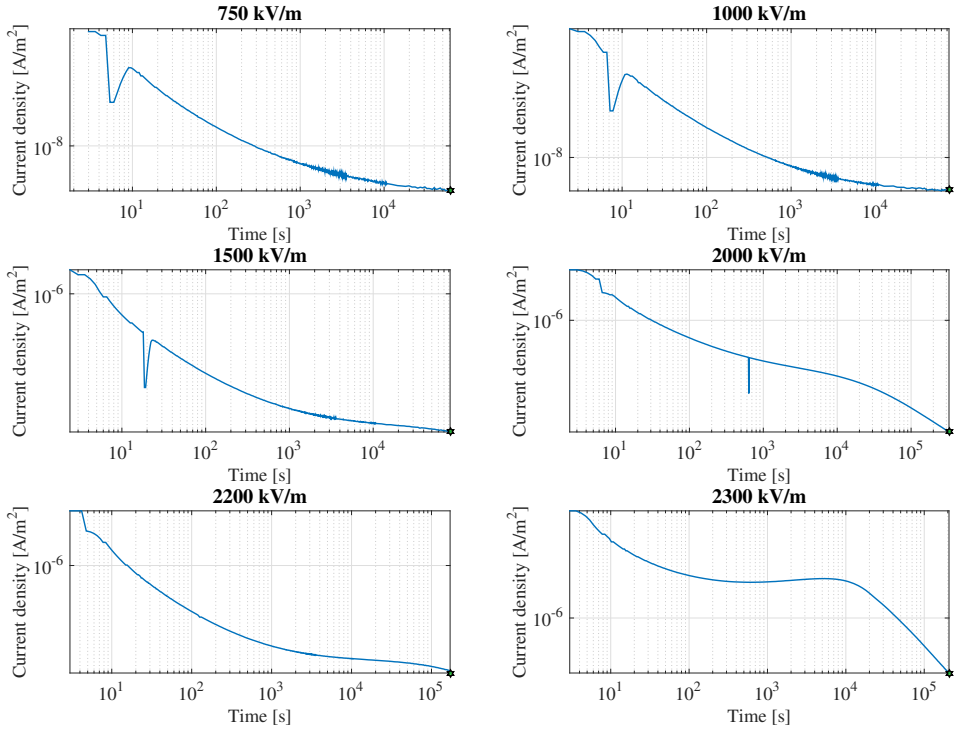

Figure B.9: Polarization currents of Material C measured with IV-setup 1 at 30 °C at different field values.

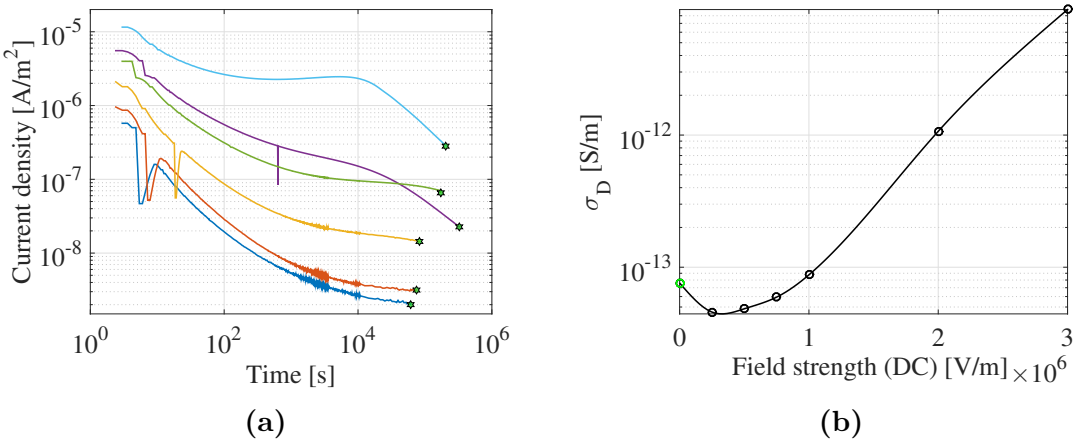

Figure B.10: Material C at 30 °C: (a) Polarization current measurements and (b) differential conductivity as a function of the DC field strength. Circles: IS measurements with small-signal AC voltage superimposed to a DC voltage (AC voltage: 3.3 V/mm (green), 23.6 V/mm (black))

Table B.3: Material C: Current density amplitudes of the fundamental frequency (j_1') in A/m^2 for different frequencies and field strengths.

Field Strength [V/m]	1 Hz	100 mHz	10 mHz	1 mHz
0.3532e06	4.2247e-06	5.8858e-07	9.1921e-08	2.1451e-08
0.7070e06	1.3154e-05	1.9371e-06	2.9359e-07	5.3387e-08
1.0565e06	3.0133e-05	4.5600e-06	7.0546e-07	1.2242e-07
1.4099e06	5.8408e-05	9.0751e-06	1.4581e-06	2.6958e-07
2.8206e06	3.6101e-04	6.7722e-05	1.6768e-05	7.4152e-06
4.2307e06	1.2610e-03	3.3652e-04	1.2658e-04	7.5316e-05

B.4 Material D

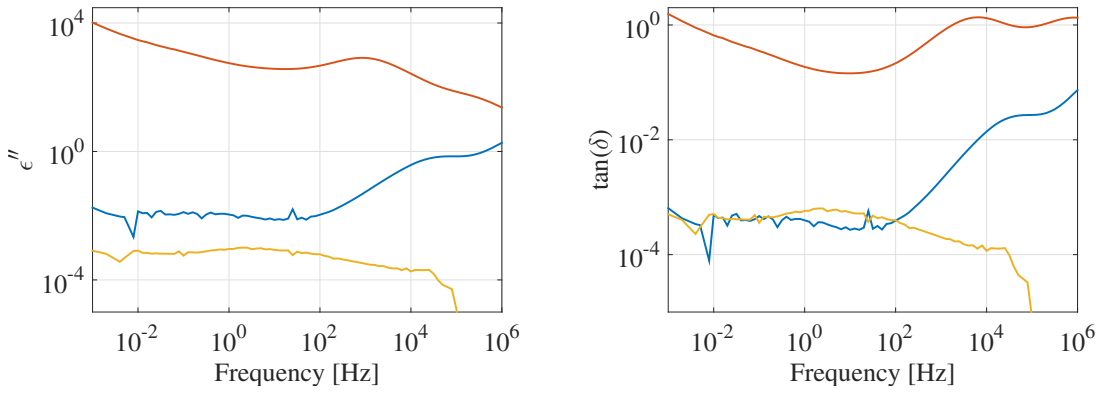

Figure B.11: The frequency behavior of the dielectric loss (ϵ'') and tan(δ) for the complete material system (blue), a Nafion sample (red) and two layers of polypropylene films (yellow) measured at a voltage of 1 V rms at 30 °C.

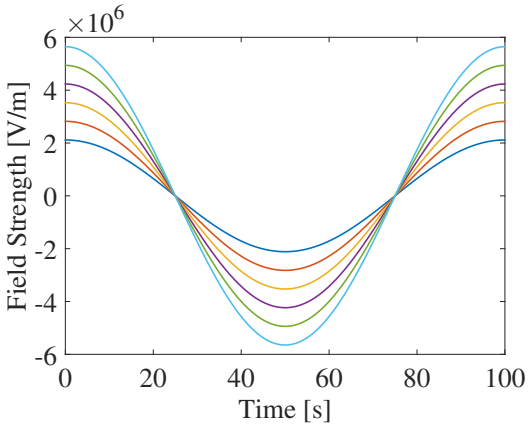

Figure B.12: Material D: Time dependent field behaviour for six different field strengths.

Table B.4: Material D: Current density amplitudes of the fundamental frequency ($j_1^{'}$) in A/m^2 for different frequencies and field strengths. The colours indicate the corresponding measurement in figure 5.17a.

Field Strength [V/m]	1 Hz (blue)	10 mHz (red)	1 Hz (yellow)	10 mHz (purple)
0.4928e06	9.3990e-06	5.8675e-08	2.8715e-07	6.0711e-08
0.7056e06	1.1303e-05	6.9180e-08	6.0480e-07	6.5398e-08
1.0572e06	1.4999e-05	1.6649e-07	8.7610e-07	8.7097e-08
1.4106e06	1.7388e-05	2.2200e-07	1.5028e-06	1.5549e-07
2.1144e06	4.5425e-05	6.4730e-07	3.5820e-06	7.1841e-07
2.8202e06	1.2576e-04	9.4021e-07	5.7084e-06	5.7275e-07
3.5250e06	1.5899e-04	6.0761e-06	2.7192e-04	9.6675e-06
4.2296e06	6.8692e-04	1.4948e-05	1.3547e-03	1.7373e-05
4.9331e06	1.6563e-03	2.3602e-05	2.3392e-03	2.4722e-05
5.6385e06	2.5651e-03	3.1096e-05	3.1945e-03	3.1505e-05